

# Hyperaccreting Disks around Magnetars for Gamma-Ray Bursts: Effects of Strong Magnetic Fields

Dong Zhang<sup>1,2</sup> and Z. G. Dai<sup>2</sup>

<sup>1</sup>*Department of Astronomy, Ohio State University, 140 W. 18th Ave., Columbus, OH  
43210;*

<sup>2</sup>*Department of Astronomy, Nanjing University, Nanjing 210093, China  
dzhang@astronomy.ohio-state.edu, dzg@nju.edu.cn*

## ABSTRACT

Hyperaccreting neutron star or magnetar disks cooled via neutrino emission can be a candidate of gamma-ray burst (GRB) central engines. The strong field  $\geq 10^{15} - 10^{16}$  G of a magnetar can play a significant role in affecting the disk properties and even lead to the funnel accretion process. In this paper we investigate the effects of strong fields on the disks around magnetars, and discuss implications of such accreting magnetar systems for GRBs and GRB-like events. We discuss quantum effects of the strong fields on the disk thermodynamics and microphysics due to modifications of the electron distribution and energy in the strong field environment, and use the magnetohydrodynamical conservation equations to describe the behavior of the disk flow coupled with a large scale field, which is generated by the star-disk interaction. If the disk field is open, the disk properties mainly depend on the ratio between  $|B_\phi/B_z|$  and  $\Omega/\Omega_K$  with  $B_\phi$  and  $B_z$  being the azimuthal and vertical components of the disk field,  $\Omega$  and  $\Omega_K$  being the accretion flow angular velocity and Keplerian velocity respectively. On the other hand, the disk properties also depend on the magnetar spin period if the disk field is closed. In general, stronger fields give higher disk densities, pressures, temperatures and neutrino luminosity. Moreover, strong fields will change the electron fraction and degeneracy state significantly. A magnetized disk is always viscously stable outside the Alfvén radius, but will be thermally unstable near the Alfvén radius where the magnetic field plays a more important role in transferring the angular momentum and heating the disk than the viscous stress. The funnel accretion process will be only important for an extremely strong field, which creates a magnetosphere inside the Alfvén radius and truncates the plane disk. Because of higher temperature and more concentrated neutrino emission of a ring-like belt region on the magnetar surface covered by funnel accretion, the neutrino annihilation rate from the accreting magnetar can be much higher than that from

an accreting neutron star without fields. Furthermore, the neutrino annihilation mechanism which releases the gravitational energy of the surrounding disk and the magnetically-driven pulsar wind which extracts the stellar rotational energy from the magnetar surface can work together to generate and feed an ultra-relativistic jet along the stellar magnetic poles.

*Subject headings:* accretion: accretion disks — black holes — gamma rays: bursts — magnetic fields — neutrinos — stars: neutron

## 1. Introduction

Hyperaccreting black hole systems formed in massive star collapses or compact object binary mergers have been considered as a candidate for gamma-ray burst (GRB) central engines for two decades (e.g., Eichler et al. 1989; Narayan et al. 1992; Woosley 1993). The accreting systems can drive ultra or mildly relativistic jets with huge energy via neutrino ( $\nu\bar{\nu}$ ) annihilation process (Popham et al. 1999) or magnetohydrodynamical (MHD) mechanism, such as the Blandford-Znajek mechanism (Blandford & Znajek 1977) or the magnetorotational instability (MRI, Balbus & Hawley 1991), and finally produce GRB explosions. The neutrino annihilation efficiency above hyperaccreting disks around black holes with the elaborate considerations of disk geometry, rotation, and general relativity effects have been studied by many authors (e.g., Ruffert et al. 1997, 1998; Popham et al. 1999; Asano & Fukuyama 2000, 2001; Miller et al. 2003; Birkel et al. 2007). Although the annihilation process can provide sufficient total energy up to  $10^{50}$  ergs  $s^{-1}$  above neutrino-dominated flows with accretion rate  $\sim 1M_{\odot} s^{-1}$  (Gu et al. 2006; Liu et al. 2007), it is still under debate whether such a process can successfully generate a relativistic jet from the polar region of the central black hole. For example, MacFadyen et al. (2001) discussed that the central black hole formed in the “collapsar scenario” is more frequent to be formed by fallback process after a mild explosion (Type II collapsar) rather than formed promptly (Type I collapsar). The Type II collapsar can establish an accretion disk with accretion rate  $\sim 0.001 - 0.01M_{\odot} s^{-1}$ , which is not sufficient to produce a jet by neutrino annihilation. Numerical simulations showed that the MHD mechanism may be more efficient to drive an energetic magnetically-dominated wind and generate a GRB explosion (Tchekhovskoy et al. 2008, 2009; Nagataki 2009), or the annihilation process and MHD winds can work together to provide the energy for GRB explosions (Harikae et al. 2009).

On the other hand, both observational and theoretical evidences show that newborn neutron stars or magnetars rather than black holes can form in the GRB central engines (e.g., Dai & Lu 1998a, 1998b; Zhang & Mészáros 2001; Dai 2004; Dai et al. 2006; Mazzali

et al. 2006; Soderberg et al. 2006; Shibata & Taniguchi 2006; Lee & Ramirez-Ruiz 2007). Highly magnetized neutron stars formed by accretion-induced-collapse, convection,  $\alpha - \Omega$  dynamo mechanism or differential rotation can extract their rotational kinetic energy up to  $\sim 10^{51} - 10^{52}$  ergs by spinning down via magnetic activities (e.g., Usov 1992; Duncan & Thompson 1992; Kluźniak & Ruderman 1998). A thermally-driven neutrino wind is dominated during the Kelvin-Helmholtz cooling epoch after the neutron star formation, lasting from a few seconds to tens of seconds based on the strengths of surface fields. After that, magnetically-dominated or Poynting-dominated wind becomes significant along the polar region (Wheeler et al. 2000; Thompson 2003; Thompson 2004; Metzger et al. 2007). The jets from magnetars may be accelerated to higher Lorentz factor  $\sim 100 - 10^3$  at large radius several tens of seconds after core bounce, and bring its magnetic energy to kinetic energy, which is finally dissipated in regular GRB internal shocks (Thompson et al. 2004; Metzger et al. 2007; Bucciantini et al. 2007, 2009; Lyubarsky 2009a, 2009b).

However, all the magnetized neutron star or magnetar models ignore the accretion process which occurs onto a protoneutron star for the first several seconds (Woosley & Bloom 2006). In the scenario of massive star collapse, the outgoing shock generated by a successful Type Ibc supernova explosion with a velocity of  $\sim 10^9$  cm s $^{-1}$  can evacuate a cavity around the new born compact star in the center of a supernova remnant. However, whether the outgoing shock in the core collapse of a massive star can dominate the accretion process and turn the accretion around is still unknown. If the rotational core collapse can lead to the formation of a neutron star or a magnetar, there is possible that the prompt accretion or fallback process can make a hyperaccreting disk around the young formed star. On the other hand, recent simulations also showed the possibility of a debris disk around a massive neutron star as the outcome of a compact binary merger (e.g., Shibata & Taniguchi 2006, Lee & Ramirez-Ruiz 2007). Similar to the black hole system, the transiently existing torus around a neutron star or magnetar with sufficient angular momentum can form a neutrino-cooled disk and release its gravitational binding energy via neutrino emission.

The hyperaccreting neutron star or magnetar system is also proposed as another possible central engine of GRBs. Zhang & Dai (2008a, 2009, hereafter papers I and II) found that, due to the inner surface boundary of the compact star, the disk has a denser, hotter inner region with higher pressure compared to its black hole counterpart. Also, the entire disk can cool more efficiently via neutrino emission and produce a higher neutrino annihilation luminosity. A heavily thermally-driven outflow from the surface of the new-born neutron star at early times ( $\sim 100$ ms) prevent the outflow from being accelerated to a high Lorentz factor (Dessart et al. 2009). However, if the disk accretion rate and the neutrino emission luminosity from the surface boundary layer are sufficiently high, an energetic ultrarelativistic jet via neutrino annihilation can be actually produced after the jet breaks out of the stellar

envelope around the disk-neutron star system.

Until now, none of the above works consider the effects of magnetic fields on the hyperaccreting transient disks around the central compact stars. The MHD mechanisms in the accreting black hole systems mainly focus on energy extraction near the central black holes, and the proto-magnetar magnetically-driven wind model discusses wind generation and propagation along the polar regions. In the hyperaccreting disk the spherical Alfvén radius of the central star can be estimated as

$$r_A \simeq 0.207 \dot{M}_{-2}^{-2/7} M_{1.4}^{-1/7} \mu_{30}^{4/7} \text{ km}, \quad (1)$$

where  $\dot{M} = 0.01 \dot{M}_{-2} M_\odot \text{ s}^{-1}$  is the accretion rate,  $M = 1.4 M_{1.4} M_\odot$  is the central star mass,  $\mu = \mu_{30} 10^{30} \text{ G cm}^3$  is the central magnetic flux. Figure 1 shows the Alfvén radius  $r_A$  as a function of accretion rate with various magnetic fields. If the surface field  $B_0$  is less than

$$B_0 \leq B_{\text{crit}} = 0.89 \times 10^{15} \dot{M}_{-2}^{1/2} M_{1.4}^{1/4} r_{*,6}^{-5/4} \text{ G} \quad (2)$$

with  $r = r_{*,6} 10^6 \text{ cm}$  being the star radius, the accretion flow will continue to be confined in the disk plane without co-rotating with the compact object or getting funneled onto the magnetar poles. Papers I and II assumed the strength of stellar surface field is less than  $10^{15} \text{ G}$ , and did not consider the effects of a magnetic field in the disk. Recently, Xie et al. (2007, 2009) and Lei et al. (2009) studied the structure of magnetized hyperaccreting neutrino-cooled disks around black holes based on similar models, while the magnetic fields are generated in the disks up to  $10^{15} - 10^{16} \text{ G}$  (see also Janiuk & Yuan 2009). Xie et al. (2007, 2009) showed that the magnetic braking and viscosity can drive magnetically-dominated accretion flows rather than neutrino-dominated, and turn the disk temperature to be lower than that without field. Lei et al. (2009) investigated the properties of the NDAF with the magnetic torque acted between the central black hole and the disk. The neutrino annihilation luminosity can be increased by one order of magnitude for accretion rate  $\sim 0.5 M_\odot \text{ s}^{-1}$ , and the disk becomes thermally and viscously unstable in the inner region. However, all of their works neglected microphysics processes and the changes of equations of state in strong magnetic fields, which may change the disk pressure and various neutrino cooling rates in the neutrino-cooled disks significantly. Furthermore, if we look into the neutron star disks, we should keep in mind that the structure of magnetic fields in disks around magnetized neutron stars or magnetars are very different from their black hole counterparts. The origin of a magnetic field in this case in the central compact star constructs the initial topology of the strong field. An interaction between the star and the surrounding disk makes the stellar magnetic field partially thread the accretion disk.

Our motivation in this paper is to investigate the effects of a strong magnetic field on the hyperaccreting disk around a magnetar formed in the collapse of a massive star or the

merger of a compact object binary, and their observational phenomena related to GRBs and associated events. The accretion process onto the magnetized neutron star has been widely studied in X-ray binaries, T Tauri stars and cataclysmic variables since Ghosh & Lamb (1978, 1979a, 1979b), both theoretically (e.g., Königl 1991; Ostriker and Shu 1995; Lovelace et al. 1995; Wang 1995; Lai 1998), and numerically (e.g., Hayashi et al. 1996; Miller & Stone 1997; Romanova et al. 2005, 2008; Long et al. 2007, 2008). The neutrino-cooled hyperaccreting disks, on the other hand, are much hotter, denser with much higher pressure and accretion rates compared to the normal disks. Therefore the structure and radiation process in these magnetized disks must be very different from the normal ones. For example, the size of the magnetosphere near the central star can be ignored except for a magnetic field  $\geq 10^{16}$  G. The pressure relation  $B^2/8\pi \gg P_{\text{matter}} + \rho v_r^2$  will not be satisfied in most cases. More attractively, we need to study the neutrino emission and annihilation process which is almost the most important properties of the hyperaccreting disks but never occur in the normal magnetized ones.

This paper is organized as follows. In Section 2 we consider the quantum effects of a strong magnetic field in the microphysical scale on disk density, pressure and various neutrino cooling rates. In Section 3, we discuss the disk conservation equations coupled with the global fields both from the central magnetar and generated via the magnetar-disk interaction. Also, we discuss the field topology of the central magnetar. Combining the equations in Section 2 and 3, we discuss the properties of the hyperaccreting disks in the strong magnetic fields numerically in Section 4. The structure of the magnetized disks depends on the detailed field strength and configuration. In Section 5.1, we further discuss the disk outflows, which may provide the kinetic energy of the supernova associated with a GRB (MacFadyen & Woosley 1999; Kohri et al. 2005). Then in Section 5.2, we describe the funnel process onto the magnetar surface when the field strength is extremely high. The funnel process will significantly affect the neutrino annihilation efficiency. Section 6 is a broad discussion. We consider the importance role played by Joule dissipation, nucleon reactions and  $r$ -process occurring in the magnetized disk, as well as various outcomes of the massive star collapse using a unified point of view. Moreover, we particularly focus on the application of magnetized hyperaccreting disks in the GRB and GRB-like events (e.g, X-ray flashes), and use a unified point of view to discuss the core collapse models related to GRBs. Conclusions are presented in Section 7.

## 2. Thermodynamics and Microphysics in Strong Magnetic Fields

### 2.1. Density and Pressure in Magnetic Fields

The distribution and energy of charged particles will change significantly if the magnetic field is greater than the critical value  $B_{ci} = m_i^2 c^3 / q_i \hbar$ , where  $m_i$  and  $q_i$  are the mass and charge of the particle respectively. As the critical value for electrons is  $B_{ce} \simeq 4.4 \times 10^{13}$  G and  $B_{cp} \simeq 1.5 \times 10^{20}$  G, we have to adopt the relativistic Dirac equation for electrons in the environment near a magnetar with the field  $B > 4.4 \times 10^{13}$  G, while the protons can be still considered as classical. The main modification of electron distribution is that, the phase space factor in the absence of the magnetic field should be replaced by the summation over possible Landau level

$$\frac{2}{h^3} \int d^3p \longrightarrow \sum_{n=0}^{\infty} g_{nL} \int \frac{eB_m}{h^2 c} dp, \quad (3)$$

where  $B_m$  is the field strength, and  $g_{nL} = 2 - \delta_{n0}$  with  $\delta_{n0}$  being the Kronecker delta function.

The electron energies are given by (Johnson & Lippmann 1949)

$$E_e = \sqrt{p^2 c^2 + m_e^2 c^4 + 2n_L e B_m \hbar c} = m_e c^2 \sqrt{x^2 + 1 + n_L b}, \quad (4)$$

where  $n$  labels the Landau level,  $b = 2e\hbar B_m / m_e^2 c^3$  is the dimensionless magnetic field parameter, and  $x = p / m_e c$  is the dimensionless momentum.

The number density of electrons and positrons with the magnetic field strength  $B_m$  is

$$\begin{aligned} n_{e^\mp} &= \sum_{n=0}^{\infty} g_{nL} \int_{-\infty}^{\infty} dp \frac{eB_m}{h^2 c} f_{e^\mp} \\ &= 2\pi \left( \frac{m_e c}{h} \right)^3 b \sum_{n=0}^{\infty} g_{nL} \int_0^{\infty} dx f_{e^\mp}, \end{aligned} \quad (5)$$

where

$$f_{e^\mp} = \frac{1}{e^{m_e c^2 \sqrt{x^2 + 1 + b n_L} / k_B T \mp \eta_e} + 1} \quad (6)$$

is the Fermi-Dirac function. The total pressure in the disk is contributed by five terms, i.e., the pressure of nucleons, electrons (including positrons), radiation, neutrino and magnetic field:

$$P = P_{\text{nuc}} + P_{\text{rad}} + P_e + P_\nu + P_B. \quad (7)$$

We take the approximation that  $P_{\text{nuc}}$  and  $P_{\text{rad}}$  do not change with magnetic fields<sup>1</sup>, and  $P_\nu = u_\nu / 3$  is only noticeable in very opaque regions in the disk, where  $u_\nu$  is the energy

---

<sup>1</sup>We neglect the photodisintegration process which happens far from the central star  $r \geq 400$  km, thus

density of neutrinos. The pressures of electrons and positrons in the strong magnetic field are

$$\begin{aligned}
 P_{e^\mp} &= \sum_{n=0}^{\infty} g_{nL} \int_{-\infty}^{\infty} dp \frac{eB_m}{3h^2} \frac{p^2 c}{\sqrt{p^2 c^2 + m_e^2 c^4 + 2n_L eB_m \hbar c}} f_{e^\mp} \\
 &= \frac{2\pi}{h^3} m_e^4 c^5 b \sum_{n=0}^{\infty} g_{nL} \int_0^{\infty} dx \frac{x^2}{\sqrt{x^2 + 1 + n_L \cdot b}} f_{e^\mp}, \tag{8}
 \end{aligned}$$

and the electron pressure  $P_e = P_{e^-} + P_{e^+}$ . The pressure of the magnetic field is  $P_B = B_m^2/8\pi$ .

If  $B \rightarrow 0$ , the number density formula (5) and (8) as a series of different Landau levels will switch back to their integral form without fields. However, the convergence performance of Landau level series becomes poor for weak magnetic fields. Figure 2 shows the convergence performance of density and pressure Landau level series, and compares the summations of formula (5) and (8) to the values without fields. Here we take temperature and chemical potential as fixed typical values in neutrino-cooled disks. We define  $b_n$  as the  $n$  term in the Landau level series of (5) and (8). We note that the value of  $b_n$  drops faster for stronger magnetic fields. So we have to take a huge number of  $b_n$  terms to calculate the summation for relatively weak magnetic fields. Moreover, whether the microphysics change in the strong fields is important also depends on the disk temperature. The difference between density or pressure with and without fields is more significant for lower temperature. This conclusion can also be applied to the hyperaccreting disks around black holes which generate the fields by MRI or differential rotation. Later in this paper, we take the upper limit  $n = 10^4$  for  $b_n$  summation calculation for  $B \geq B_{ce}$ , as the pressure or the equations of state in a magnetized disk switch back to those without fields for  $B < B_{ce}$  and the typical temperature in the disks.

## 2.2. Neutrino Cooling in Magnetic Fields

Neutrino cooling processes (especially, the Urca process) in the environment of compact object magnetic fields have been studied for years (e.g., Chen et al. 1974; Dorofeev et al. 1985; Dai et al. 1993; Yuan & Zhang 1998; Lai & Qian 1998; Roulet 1998; Baiko & Yakovlev 1999; Yakovlev et al. 2001; Duan & Qian 2004, 2005; Luo 2005; Riquelme et al. 2005). Similarly, strong magnetic fields also affect the neutrino emission in a hyperaccreting disk around the compact object. Here we consider the problem systematically in this section.

---

the nucleons are mainly composed of classical protons and neutrons without  $\alpha$ -particles in the disk region we focus on. The equations of state for protons and neutrons do not change with field  $B < 10^{20}$  G as mentioned above.

The total neutrino cooling rates in the vertically-integrated disk are taken as (Di Matteo et al. 2002; Kohri et al. 2005)

$$Q_\nu^- = \sum_{i=e,\mu,\tau} \frac{(7/8)\sigma_B T^4}{(3/4)[\tau_{\nu_i}/2 + 1/\sqrt{3} + 1/(3\tau_{a,\nu_i})]}, \quad (9)$$

where the total optical depth for three types of neutrinos  $\tau_{\nu_i} = \tau_{a,\nu_i} + \tau_{s,\nu_i}$  with  $\tau_{a,\nu_i}$  being the absorption depth and  $\tau_{s,\nu_i}$  the scattering depth, both of which can be affected by strong magnetic fields.

The neutrino absorption depth can be approximately given by (Popham et al. 1999)  $\tau_{a,\nu_i} = \dot{q}_{a,\nu_i} H / (\frac{7}{2}\sigma_B T^4)$ , where  $\dot{q}_{a,\nu_i}$  are the absorption neutrino cooling rates for three types of neutrino, and  $H$  is the half thickness of the disk. The electron neutrino cooling rate  $\dot{q}_{a,\nu_e}$  in the disk can be simply taken as the summation of four terms  $\dot{q}_{a,\nu_e} = (\dot{q}_{eN} + \dot{q}_{e^-e^+\rightarrow\nu_e\bar{\nu}_e} + \dot{q}_{\text{brems}} + \dot{q}_{\text{plamson}})H$ , which are the the cooling rates due to electron-positron capture by nucleons, electron-positron pair annihilation into neutrinos, nucleon-nucleon bremsstrahlung, and plasmon decays respectively (Kohri & Mineshige 2002). On the other hand, the muon and tau neutrino cooling rates are the summations of pair annihilation and bremsstrahlung  $\dot{q}_{a,\nu_\mu} H = \dot{q}_{a,\nu_\tau} H \simeq (\dot{q}_{e^-e^+\rightarrow\nu_\tau\bar{\nu}_\tau} + \dot{q}_{\text{brems}})H$ .

The neutrino cooling via electron-positron capture by nucleons (or say the Urca process in the disk), which is usually the most significant cooling rate among various cooling terms in hyperaccreting disks, can be considered as the combination of three processes:  $\dot{q}_{eN} = \dot{q}_{p+e^-\rightarrow n+\nu_e} + \dot{q}_{n+e^+\rightarrow p+\bar{\nu}_e} + \dot{q}_{n\rightarrow p+e^-\bar{\nu}_e}$ . If we take the parameter  $\tilde{K}$  as

$$\tilde{K} = \frac{G_F^2 C_V^2 (1 + 3g_A^2)}{\pi^3 \hbar^7} (m_e c)^6, \quad (10)$$

where  $G_F^2 \simeq 1.436 \times 10^{-49}$  ergs cm<sup>-3</sup>,  $C_V = 1/2 + 2\sin^2\theta_W$  with  $\sin^2\theta_W = 0.23$ , and  $g_A = -1.23$ . Using the modification rule in strong fields (3), we can obtain the three terms of neutrino cooling rates in strong magnetic fields as

$$\dot{q}_{p+e^-\rightarrow n+\nu_e} = b \frac{\tilde{K}}{4} \sum_{n=0}^{\infty} g_{nL} n_p \int_{\max\{q, \sqrt{1+nLb}\}}^{\infty} \frac{\varepsilon(\varepsilon - q)^3 d\varepsilon}{\sqrt{\varepsilon^2 - 1 - nLb}} f_{e^-}, \quad (11)$$

$$\dot{q}_{n+e^+\rightarrow p+\bar{\nu}_e} = b \frac{\tilde{K}}{4} \sum_{n=0}^{\infty} g_{nL} n_n \int_{\sqrt{1+nLb}}^{\infty} \frac{\varepsilon(\varepsilon + q)^3 d\varepsilon}{\sqrt{\varepsilon^2 - 1 - nLb}} f_{e^+}, \quad (12)$$

$$\dot{q}_{n\rightarrow p+e^-\bar{\nu}_e} = b \frac{\tilde{K}}{4} \sum_{n=0}^{\infty} g_{nL} n_n \int_{\sqrt{1+nLb}}^q \frac{\varepsilon(q - \varepsilon)^3 d\varepsilon}{\sqrt{\varepsilon^2 - 1 - nLb}} (1 - f_{e^-}), \quad (13)$$

where  $\varepsilon = E_{\nu_e}/m_e c^2$  is the dimensionless energy of electrons, and  $q = (m_n - m_p)/m_e \approx 2.531$ . Here we adopt the approximation adopted in Shapiro & Teukolsky (1983) that the total reaction on nucleons is directly proportional to the density number of nucleons, i.e., protons and neutrons. Figure 3 shows the convergence performance of Landau level series of two dominated cooling rates (11) and (12) with the typical temperature and chemical potential in neutrino-cooled hyperaccreting disks. Similar to the density and pressure in a strong magnetic field, the convergence properties of neutrino cooling series also go poorer for a weaker field. Moreover, the total Urca neutrino cooling rate becomes lower for a higher magnetic field. Although the difference is not significant for  $T = 5 \times 10^{10}$  K, it can be greater for a lower temperature, as shown in Figure 2. We will discuss this effect later in Sections 4 and 6.

The electron-positron pair annihilation rate without magnetic fields can be calculated as (Burrows & Thompson 2004)

$$\dot{q}_{e^-e^+ \rightarrow \nu_e \bar{\nu}_e} \simeq \dot{q}_{\nu_e \bar{\nu}_e(B=0)} \simeq 2.558 \times 10^{33} T_{11}^9 f(\eta_e) \text{ ergs cm}^{-3} \text{ s}^{-1}, \quad (14)$$

$$\dot{q}_{e^-e^+ \rightarrow \nu_\mu \bar{\nu}_\mu} = \dot{q}_{e^-e^+ \rightarrow \nu_\tau \bar{\nu}_\tau} \simeq 1.093 \times 10^{33} T_{11}^9 f(\eta_e) \text{ ergs cm}^{-3} \text{ s}^{-1}, \quad (15)$$

where the function  $f(\eta_e)$  is

$$f(\eta_e) = \frac{F_4(\eta_e)F_3(-\eta_e) + F_4(-\eta_e)F_3(\eta_e)}{2F_4(0)F_3(0)} \quad (16)$$

with the function  $F_n(\pm\eta_e)$  being

$$F_n(\pm\eta_e) = \int_0^\infty \frac{x^n}{e^{x \mp \eta_e} + 1} dx. \quad (17)$$

In the case of strong magnetic fields, we can approximately take the annihilation rate as

$$\dot{q}_{\nu_i \bar{\nu}_i} = \dot{q}_{\nu_i \bar{\nu}_i(B=0)} \times \frac{B_m e \hbar m_e^2 c^5}{28 \pi^2 T^4 k_B^4}, \quad (18)$$

when the field strength  $B_m$  satisfies  $B_m \hbar e c \gg T^2 k_B^2$  (e.g., Kaminker et al. 1992; Yakovlev et al. 2001).

In most cases the cooling processes via bremsstrahlung and plasmon decay are much less significant than  $e^-e^+$  capture and annihilation, furthermore the unchanged distribution and energy of neutrons and photons. Therefore we still use the formulae as in Kohri et al. (2005) for these two processes.

Besides the absorption depth, three types of optical depth for neutrinos through scattering off nucleons and electrons are given by

$$\begin{aligned} \tau_{s, \nu_i} &= (\sigma_{\nu_i p} n_p + \sigma_{\nu_i n} n_n + \sigma_{\nu_i e} n_e) H \\ &= (\sigma_{\nu_i p} Y_p + \sigma_{\nu_i n} Y_n + \sigma_{\nu_i e} Y_e) \rho H / m_B, \end{aligned} \quad (19)$$

where  $\sigma_{\nu_i p}$ ,  $\sigma_{\nu_i n}$  and  $\sigma_{\nu_i e}$  are the cross sections of scattering on protons, neutrons and electrons,  $\rho$  is the density of the disk. We take the cross sections of  $\sigma_{\nu_i p}$  and  $\sigma_{\nu_i n}$  in strong magnetic fields as

$$\sigma_{\nu_i p} \simeq \sigma_{\nu_i p(B=0)} = \frac{\sigma_0}{6} \left( \frac{\varepsilon_\nu}{m_e c^2} \right)^2 [(C_V - 1)^2 + 5g_A^2(C_A - 1)^2], \quad (20)$$

$$\sigma_{\nu_i n} \simeq \sigma_{\nu_i n(B=0)} = \frac{\sigma_0}{4} \left( \frac{\varepsilon_\nu}{m_e c^2} \right)^2 \left( \frac{1 + 5g_A^2}{6} \right), \quad (21)$$

which are still classical (Tubbs & Schramm 1975; Burrows & Thompson 2004). Here  $\sigma_0 \simeq 1.705 \times 10^{-44} \text{ cm}^2$  is the neutrino cross section coefficient. On the other hand, neutrino-electron scattering process in a strong magnetic field has been discussed by many authors using various approaches (e.g., Bezchastnov & Haensel 1996; Kuznetsov & Mikheev 1997, 1999; Hardy & Thoma 2000; Mikheev & Narynskaya 2000). Although the analytic results are quite complicated and different based on various approximated treatments, all of these works show that the cross section  $\sigma_{\nu_i e}$  is proportional to the field strength  $\propto eB_m$ . For simplicity, we use the factor  $2eB_m \hbar c / (k_B T)^2$  to compare the importance of electron energies in strong fields and the thermal energy, and consider the cross section  $\sigma_{\nu_i e}$  in strong magnetic fields as

$$\sigma_{\nu_i e} \simeq \sigma_{\nu_i e(B=0)} \times [1 + 2eB_m \hbar c / (k_B T)^2] \quad (22)$$

with

$$\sigma_{\nu_i e(B=0)} = \frac{3\sigma_0}{8} \left( \frac{k_B T}{m_e c^2} \right) \left( \frac{\varepsilon_\nu}{m_e c^2} \right) \left( 1 + \frac{\eta_e}{4} \right) [(C_V + C_A)^2 + (C_V - C_A)^2 / 3]. \quad (23)$$

### 3. Conservation Equations in Magnetized Disks and Field Topology

#### 3.1. Conservation Equations

In Section 2 we discussed the microphysics and thermodynamics equations in strong magnetic fields, and compare them with the equations without fields. Now we consider the basic conservation magnetohydrodynamical (MHD) equations for a vertically-integrated steady-state magnetized disk. We modify the hydrodynamical equations without fields by adding the coupling of a large-scale magnetic field. In this case we consider the accretion flow is still constrained in the disk plane. The disk with an outflow structure will be discussed in Section 5.1, and the funnel accretion process in an extremely strong field in the stellar magnetosphere will be discussed in Section 5.2. First of all, the mass continuity equation in a vertically-integrated disk does not change

$$\dot{M} = -2\pi r \Sigma v_r, \quad (24)$$

where  $\Sigma = 2\rho H$  is the disk surface density and  $v_r$  is the radial velocity of the accretion flow.

The vertically-integrating angular momentum conservation equation with fields reads (e.g., Lovelace et al. 1987; Shadmehri & Khajenabi 2005)

$$\dot{M} \frac{dl}{dr} = -2\pi \frac{d}{dr} \left( r^3 \Sigma \nu \frac{d\Omega}{dr} \right) - r^2 B_z B_\phi|_{z=H} + \frac{dH}{dr} (r^2 B_r B_\phi)|_{z=H} - \frac{d}{dr} (H r^2 \langle B_r B_\phi \rangle), \quad (25)$$

where  $\langle \dots \rangle = \int_{-H}^H dz(\dots)/2h$ ,  $\nu = \alpha c_s H$  is the kinematic viscosity coefficient in the disk with  $\alpha$  being the viscosity parameter. Here we still use the  $\alpha$ -prescription<sup>2</sup>. The magnetic field can play an important role in transferring the angular momentum. If the radial field  $B_r$  can be neglected (as will be shown in Section 3.2), we can integrate the angular momentum equation as

$$\frac{\dot{M}}{3\pi} f = \nu \Sigma - \frac{\dot{M} N_B}{3\pi r^2 \Omega}, \quad (26)$$

where

$$\dot{M} N_B(r) = - \int_r^\infty r^2 B_z B_\phi|_{z=H} dr \quad (27)$$

is the integrated magnetic torque,  $f = 1 - l_0/(r^2 \Omega)$  with  $l_0$  being the specific angular momentum constant. In the standard assumption that the viscous torque is zero at the inner boundary of the disk  $r_* + b$  with  $r_*$  being the stellar radius and  $b \ll r_*$ , we can take  $f = 1 - \sqrt{r_*/r}$  (Frank et al. 2002).

The local energy conservation equation in a magnetized disk is

$$Q_{\text{vis}}^+ + Q_{\text{Joule}}^+ = Q_{\text{adv}}^- + Q_\nu^-, \quad (28)$$

where  $Q_{\text{vis}}^+$  and  $Q_{\text{adv}}^-$  keep the same as in the case of  $B_m = 0$  ((A12) and (A13) in Appendix A), and the neutrino cooling rate  $Q_\nu^-$  in strong magnetic fields have been discussed in Section 2.2. In particular, the Joule dissipation (or say the Joule heating) term  $Q_{\text{Joule}}^+$  is

$$\begin{aligned} Q_{\text{Joule}}^+ &= \frac{4\pi H}{c^2} \eta_t \langle J^2 \rangle = \frac{H}{4\pi} \eta_t \langle (\nabla \times B_m)^2 \rangle \\ &\simeq \frac{H \eta_t}{4\pi} \left\{ -\frac{2B_r|_{z=H}}{H} \frac{\partial B_z}{\partial r} \Big|_{z=H} + \left( \frac{\partial B_z}{\partial r} \right)^2 + \frac{1}{r^2} \left[ \frac{\partial(rB_\phi)}{\partial r} \right]^2 \right\}, \quad (29) \end{aligned}$$

---

<sup>2</sup>Actually, the half thickness of the disk  $H$  and the kinematic viscosity  $\nu = \alpha c_s H$  will change depending on the field structure. For example, the half thickness  $H$  will increase for large  $B_\phi$  if  $B_r \ll B_\phi, B_z$  (Zhang & Dai 2008b). Also, Shakura & Sunyaev's scenario (1973)  $\nu = \alpha c_s^2 / \Omega_K$  should be modified as  $\nu = \alpha' c_s^2 / \Omega_K$  with  $\alpha'$  being the function of magnetic fields. In this paper we use the following treatment: calculate the magnetic pressure  $P_B$  into the total pressure, since the isothermal sound speed  $c_s \propto P^{1/2}$ ,  $c_s$  and the disk half thickness can increase for strong fields. We still adopt the classical relation  $H = c_s / \Omega_K$  and  $\nu = \alpha c_s^2 / \Omega_K$  for simplicity.

where the magnetic diffusivity parameter  $\eta_t$  is adopted as  $\eta_t \sim \nu \simeq \alpha c_s H$  (Lovelace et al. 1995; Bisnovatyi-Kogan & Lovelace 1998). In Section 6.1, we will discuss the Joule dissipation term in more details.

Moreover, we need to add the charge conservation equation and the chemical equilibrium equation, which are the same in paper II (or see Appendix A (A7) and (A14)).

### 3.2. Field Topology

The magnetic field of a neutron star or magnetar threading the disk has the vertical component

$$B_z(r) = B_0 \left( \frac{r_*}{r} \right)^n. \quad (30)$$

The actual magnetic field in the vertical component near a magnetar may be a mix of monopole ( $n = 2$ ) and dipole ( $n = 3$ ) fields (Thompson et al. 2004). The dipole field drops faster than the monopole field along the disk radius, thus the disk properties will be quite different with the other cases. We focus on the dipolar form  $n = 3$  in this paper.

The differential rotation between the disk and the star will generate a toroidal field (Wang et al. 1995). Following Lai (1998), we consider two possible field configurations in a disk, i.e., the stellar magnetic field threads the accretion disk in a closed configuration (i.e., the classical configuration as in Ghosh & Lamb 1979a), or the magnetic field becomes open (e.g., Lovelace et al. 1995). The generated azimuthal component of the magnetic field in a steady-state disk is

$$B_\phi|_{z=H} = -\beta B_z \quad (31)$$

for an open magnetic field in the disk, and

$$B_\phi|_{z=H} = -\beta \left( \frac{\Omega - \Omega_*}{\Omega_K} \right) B_z \quad (32)$$

for a closed magnetic field, where  $\beta$  is a dimensionless parameter,  $\Omega_*$  and  $\Omega_K$  are the stellar surface angular velocity and Kepler velocity respectively. The radial component  $B_r$  generated in the disk reads

$$B_r|_{z=H} \propto \left( \frac{-v_r}{\Omega_K r} \right) B_z|_{z=H} \quad (33)$$

In most cases, we consider  $v_r \ll v_K = \Omega_K r$  and  $B_r|_{z=H} \ll B_z|_{z=H}$ . Thus the field strength  $B_m$  in the disk can be obtained as  $B_m = \sqrt{B_z^2 + B_\phi^2 + B_r^2} \approx \sqrt{B_z^2 + B_\phi^2}$ .

According to Lovelace et al. (1995), if the angular velocities of the star and disk differ substantially, the magnetic field lines threading the star and the disk undergo a rapid inflation

so that the field becomes open. As a result, the outer part of the disk will maintain an open field configuration, while the inner disk in the magnetosphere still has closed lines. Since in the hyperaccreting case the magnetosphere is very small except for an extremely strong center field, in which the disk plane will be disrupted and truncated in the magnetosphere (see discussion in Section 5), the magnetized disk where still has a plane geometry would be more favorable to maintain an open field. However, we still consider the two cases as a broader consideration. If the magnetic field in the disk is open, the magnetic torque in equation (26) becomes

$$\dot{M}N_B = \beta B_z^2 \frac{r^3}{2n-3}, \quad (34)$$

and the integrated angular momentum equation (26) can be written as

$$\frac{GM\dot{M}}{3\pi} f + \frac{1}{3\pi} \frac{\beta}{s} \sqrt{GM} B_z^2 \frac{r^{5/2}}{2n-3} = 2\alpha \frac{P^{3/2}}{\rho^{1/2}} r^3, \quad (35)$$

where we take the ratio of the angular velocity of the disk flow and the Keplerian velocity as a constant  $s = \Omega/\Omega_K$ . For the case of a closed disk field, on the other hand, using (32) we have

$$\dot{M}N_B = \beta s B_z^2 \frac{r^3}{2n-3} - \beta \Omega_* B_z^2 (GM)^{-1/2} \frac{r^{9/2}}{2n-9/2} \quad (36)$$

and the angular momentum equation (26) reads

$$\frac{GM\dot{M}}{3\pi} f + \frac{\sqrt{GM}}{3\pi} \frac{\beta}{2n-3} B_z^2 r^{5/2} - \frac{2\beta}{3s} \frac{B_z^2 r^4}{P_r} \frac{1}{2n-9/2} = 2\alpha \frac{P^{3/2}}{\rho^{1/2}} r^3, \quad (37)$$

where  $P_r$  is the spin period of the magnetar.

Moreover, we obtain the energy conservation equation (28) in disk with the detailed field topology structure as

$$\frac{3GM\dot{M}}{8\pi r^3} f + \frac{H\eta_t}{4\pi r^2} [n^2 + (n-1)^2 \beta^2] B_z^2 = Q_{\text{adv}}^- + Q_\nu^- \quad (38)$$

for an open magnetic field, and

$$\frac{3GM\dot{M}}{8\pi r^3} f + \frac{H\eta_t}{4\pi r^2} \left\{ n^2 + \left[ s(n-1) - \frac{\Omega_*}{\Omega_K} \left( n - \frac{5}{2} \right) \right]^2 \beta^2 \right\} B_z^2 = Q_{\text{adv}}^- + Q_\nu^- \quad (39)$$

for a closed field.

We make a brief summary in the end of this section. We consider the quantum effects of strong fields on the disk thermodynamics and microphysics in Section 2.1, and the MHD conservation equation with coupling of a large scale disk field in Section 2.2. The strong

magnetic field can change the electron distribution and energy significantly, and also change the cross sections of the various neutrino reactions. The large scale field can play an important role in transferring angular momentum besides the viscous stress, and heat the disk as well. In order to see the differences of disks with and without field (or more exactly to say, with fields  $\leq 10^{14}$  G in the hyperaccreting disk) clearly, we list the basic equations without fields in Append A for a comparison.

#### 4. Numerical Solutions of Magnetized Neutrino-Cooled Disks

We adopt the  $\alpha$  turbulent viscosity model of Shakura & Sunyaev (1973) and fix  $\alpha = 0.1$  in all of our calculations. First we want to study the direct quantum effects of strong magnetic fields on the disk, and the macrophysical field coupling in the MHD conservation equations independently. Figure 4 and Figure 5 give the independent results. In Figure 4, we keep the conservation equations as the normal hydrodynamical equations without fields (i.e., equations (A8), (A10) to (A14) in the Appendix), and only adopt the equations of state (4) to (23) in Section 2 to see the quantum effects of a field. On the other hand, in Figure 5, we keep the microphysical and thermodynamical equations as in the case of no field (i.e., equations (A1) to (A7) in Appendix A and the equations in Section 2 without fields), but only discuss the field effect on angular momentum transfer (26) and energy heating (28). As discussed by Duncan & Thompson (1992), in principle the magnetic fields as strong as  $3 \times 10^{17}(P/\text{ms})^{-1}$  G can be generated in magnetars as the differential rotation smoothed by growing magnetic stresses. Kluźniak & Ruderman (1998, see also Ruderman et al. 2000) argued that the energy stored in the differentially-rotating magnetars can be extracted by the process of wounding up and amplification of toroidal magnetic fields inside the star up to  $\sim 10^{17}$  G, then the ultra strong field will be pushed to and through the surface by buoyancy force. Based on these considerations, we adopt the magnetar surface field up to  $\sim 10^{17}$  G, and discuss the field strength from  $10^{14}$  G to  $10^{17}$  G with a dipolar extension in our calculations. The steady state disk can be considered as the transient hyperaccreting disk with a fixed time, or say, with a fixed accretion rate. On the contrary, for a time-dependent disk model (e.g., Janiuk et al. 2004, 2007 without fields), we have to consider the evolution of the magnetar surface field, which is beyond the purpose of this paper. Moreover, we do not consider other quantum processes in strong fields such as the generation of strong electric field and electron/positron pairs as  $E \rightarrow e^- + e^+ + E$  and  $\gamma + B \rightarrow e^- + e^+ + B$  (Usov 1992). These processes are important in the pulsar magnetosphere, but plays a secondary role in the disk region outside the Alfvén radius. In Figure 4, a stronger magnetic field makes the disk be thinner, cooler with lower temperature and neutrino luminosity. On the contrary, Figure 5 shows that the disk will be denser with higher pressure and neutrino luminosity,

and becomes hotter at least in the inner disk region near the magnetar, because the stronger field plays a more significant role in transporting the disk angular momentum and heating disk by Joule dissipation<sup>3</sup>. As a result, the quantum effects in strong fields and the field coupling in MHD equations play two opposite roles in changing the disk properties, one to decrease pressure, density and luminosity with increasing field strength, and the other to increase them. These two competitive factors work together to establish the actual structure of the disk.

In Figure 6 we consider the quantum and coupling effects together. This figure is for the disk structure and neutrino luminosity with accretion rate  $\dot{M} = 0.1M_{\odot} \text{ s}^{-1}$  and an open magnetic field configuration in the disk. From equation (35) we know that the ratio between the two parameters  $\beta/s$  determines the angular momentum transfer by magnetic field. As the result of Figure 6, a higher ratio of  $\beta/s$  leads to a higher density and pressure in the entire disk, higher temperature and neutrino luminosity in the inner region of the disk, as well as lower electron fraction at the disk radius  $\sim 30$  km. Moreover, electrons in the disk becomes more degeneracy around  $\sim 20 - 40$  km for higher  $\beta/s$ , but quickly changes to be nondegeneracy at the inner edge of the disk toward the magnetar surface.

Figure 7 gives the magnetized disk for various surface vertical field  $B_0$  and open magnetic field configuration in the disk. Stronger fields give higher density, pressure, temperature and neutrino luminosity. This figure shows that the magnetic field coupling in the MHD equations of disk flow is more important than the quantum effects of strong fields in a microphysical scale. In the case of  $B_0 = 10^{17}$  G, the disk has no steady state solution in the inner region of the disk where the flow should co-rotate with the central star and further be channeled onto the magnetic pole along the field lines. We will discuss the funneled flows later. On the other hand, for  $B_0 = 10^{14}$  G, we stop calculation where the disk field is too weak for us to consider the quantum effect in strong fields as discussed in Section 2. In this case, the disk properties will be very similar to the case of  $B_0 = 10^{14}$  G without quantum effect even in the case of  $B_0 = 0$ , which has been showed in Figure 5. The electron fraction decreases inward for  $B \leq 10^{16}$  G, which is similar to the results without fields (e.g., paper I, Fig. 7), but a field  $\sim 10^{17}$  G will change the electron fraction distribution significantly. The distribution of electron potential  $\eta_e$  along the radius also changes a lot in strong fields. Larger peak with more degeneracy electron state is obtained by stronger fields, while the change of  $\eta_e$  becomes less obvious for relatively weaker fields.

---

<sup>3</sup>In this section, we extend our calculation to the inner disk region inside the Alfvén radius  $r_A$ . This extension is good for us to see the disk properties of magnetized disks, although we need to use another treatment to discuss the disk structure in the magnetosphere with an extreme strong field.

Above we focus on the disk accretion rate of  $\sim 0.1M_{\odot} \text{ s}^{-1}$ , which is typical for a magnetar hyperaccreting disk. Moreover generally, we can study the magnetized disks with different accretion rates. We discuss the disk properties with open disk field and different accretion rate  $\dot{M} = 0.02, 0.1$  and  $1 M_{\odot} \text{ s}^{-1}$  in Figure 8. The values of density, pressure temperature and neutrino luminosity become higher for higher accretion rate. This result is similar to the case without field. Also, lower electron fraction and more degeneracy electron state can be obtained for higher accretion rate, except for the inner region where the Joule dissipation becomes more significant than the viscous heating. Therefore, the accretion rate plays a very similar role in changing the disk properties to that without fields. However, we should point out that, there is no steady-state solution for  $\dot{M} = 0.02M_{\odot} \text{ s}^{-1}$  in the inner disk region  $B_0 = 10^{16} \text{ G}$ . This is reasonable and similar to the case of  $\dot{M} = 0.1M_{\odot} \text{ s}^{-1}$  and  $B_0 = 10^{17} \text{ G}$ , as such a region is already inside the Alfvén radius and is almost belong to the magnetosphere. The extension calculation in this section cannot reach this region.

Figure 9 shows the disk structure for a closed magnetic field in the disk. We discuss it besides the open disk field configuration for completeness. In this case, the disk properties not only depend on the disk field structure ( $\beta$ ) and angular velocity ( $s$ ), but also depend on the spin period of the central magnetar. A normal pulsar has a spin period around  $1 \text{ s} \sim 100 \text{ s}$ , while the new born pulsar as a candidate for GRB central engines usually has a much shorter period with a timescale about tens of milliseconds or even less. Here we consider the magnetar with a period  $P_r = 5, 10, 100 \text{ ms}$ . A rapidly rotating magnetar can act an extra torque on the disk. However, we only consider the magnetic field torques from the magnetar for simplicity. A shorter period of the central magnetar decreases the disk density, pressure and electronic chemical potential slightly, but increases the temperature at  $20 - 40 \text{ km}$  and the electron fraction at  $r \geq 20 \text{ km}$  (note that there is a peak of  $\eta_e$ ) at  $r = 20 \text{ km}$  for  $B_0 = 10^{16} \text{ G}$ . The effects of period change on the disk are only obvious for the surface vertical field  $B_0 \geq 10^{16} \text{ G}$  in Figure 9. However, since the neutrino luminosity does not change significantly even for  $B_0 \simeq 10^{16} \text{ G}$ , we cannot expect any obvious observational events from the disk plane related to the effect of period on the disks directly.

Figure 10 shows the  $\dot{M} - \Sigma$  curves for a given disk radius  $r = 40$  and  $80 \text{ km}$ . In order to see the stable performance clearly, we extend our calculation to  $\dot{M} = 10M_{\odot} \text{ s}^{-1}$ , although such an accretion rate is impossible for an accreting magnetar system. The condition for viscous stability is  $d\dot{M}/d\Sigma > 0$ . Therefore the disk is viscously stable for  $B_0 \leq 10^{16} \text{ G}$ , but becomes unstable in the inner region  $r \leq 40 \text{ km}$  for  $B_0 \sim 10^{17} \text{ G}$  with both open and closed disk fields until  $\dot{M} \geq 1M_{\odot} \text{ s}^{-1}$ . However, because the Alfvén radius  $r_A \gg 40 \text{ km}$  for  $\dot{M} \leq 1M_{\odot} \text{ s}^{-1}$  and  $B_0 \sim 10^{17} \text{ G}$ , such an entire instable region actually interacts in the stellar magnetosphere. Therefore we can conclude that the accretion flow in the disk plane can always be viscously stable. This conclusion is consistent with that in the case of no fields

(Narayan et al. 2001; Di Matteo et al. 2002; Kawanaka & Mineshige 2007), but is somewhat different to that in Lei et al. (2009), who showed that the disk is always unstable in the inner disk region. The main difference is caused by different magnetic structures between neutron star disks and their black hole counterparts.

The black hole hyperaccreting disk without fields is thermally stable, at least in the region where the nucleon gas pressure dominates over the total pressure (Narayan et al. 2001; Di Matteo et al. 2002, Kawanaka & Mineshige 2007). However, a magnetic field in the disk can make the disk be thermally unstable. We roughly estimate it with an analytic method. The general condition for thermal stability can be taken as (Narayan et al. 2001)  $(d\ln Q^+ / d\ln H)|_\Sigma < (d\ln Q^- / d\ln H)|_\Sigma$ . The ratio of viscous and Joule heating is

$$\frac{Q_{\text{vis}}^+}{Q_{\text{Joule}}^+} \propto \frac{GM\dot{M}f}{rH\eta_t B_z^2} \propto \frac{\nu\Sigma}{\eta_t H} \propto H^{-1}, \quad (40)$$

As a result we have

$$\frac{d\ln Q_{\text{vis}}^+}{d\ln H}|_\Sigma < \frac{d\ln Q^+}{d\ln H}|_\Sigma < 1 + \frac{d\ln Q_{\text{vis}}^+}{d\ln H}|_\Sigma, \quad (41)$$

i.e., the value of  $(d\ln Q^+ / d\ln H)|_\Sigma$  increases by unity if  $Q_{\text{Joul}}^+$  dominates over  $Q_{\text{vis}}^+$  in the magnetized disk. Now we calculate the ratio  $(d\ln Q_{\text{vis}}^+ / d\ln H)|_\Sigma$  in the magnetized disk. Taking the open field configuration as an example. The ratio of angular momentum transferred by magnetic torque and viscous stress is

$$\frac{\dot{J}_m}{\dot{J}_{\text{vis}}} = \frac{\beta}{s(2n-3)} \frac{B_z^2}{\sqrt{GM\dot{M}f}} \frac{r_*^6}{r^{7/2}} = 12.3\beta s^{-1} M_{1.4}^{-1/2} M_{-1}^{-1} f^{-1} r_{*,6}^6 r_6^{-7/2} B_{0,16}^2. \quad (42)$$

Furthermore

$$\frac{d\ln Q_{\text{vis}}^+}{d\ln H}|_\Sigma = 2 \left( 1 + \frac{\dot{J}_m}{\dot{J}_{\text{vis}}} \right) = 2 + 24.6\beta s^{-1} M_{1.4}^{-1/2} M_{-1}^{-1} f^{-1} r_{*,6}^6 r_6^{-7/2} B_{0,16}^2. \quad (43)$$

We can see that in the outer part of the disk, the ratio (43) is still  $\simeq 2$ , but it can be significant increased in the disk inner part where the magnetic field is sufficiently high. If we take the radius  $r \simeq r_A$  or  $r_6 \simeq 2\dot{M}_{-1}^{-2/7} M_{1.4}^{-1/7} B_{0,16}^{4/7} r_{*,6}^{12/7}$ , equation (43) becomes

$$\frac{d\ln Q_{\text{vis}}^+}{d\ln H}|_\Sigma \simeq 2 + 2.174\beta s^{-1} (1 - 0.707\dot{M}_{-1}^{1/7} B_{0,16}^{-2/7})^{-1}. \quad (44)$$

On the other hand, for the neutrino-cooled region, the neutrino cooling rate under strong fields can be approximately taken as  $Q_\nu^- \propto \Sigma T^4 \propto H^8$ , or  $(d\ln Q^- / d\ln H)|_\Sigma \simeq 8$ . Based on the above calculation, whether the gas dominated disk region is thermally stable or not depends on the disk radius, magnetic field strength, disk angular velocity and accretion

rate. For typical values  $\beta \sim s$ ,  $\dot{M}_{-1} = 1$ ,  $B_{0,16} = 1$ , and  $r$  is comparable to  $r_A$ , we have  $(d\ln Q^+/d\ln H)|_\Sigma \simeq 10.4$ , which shows a thermally unstable performance. Furthermore, The radiation dominated region of accretion disks are expected to be thermally unstable in the  $\alpha$ -model without a large-scale field (Lightman & Eardley 1974; Shakura & Sunyaev 1973; Narayan et al. 2001), therefore such a region in the magnetized disk around a magnetar will be always thermally unstable. On the other hand, Hirose, Krolik & Blaes (2009) showed the disk thermal stability based on the 3-dimensional radiation MHD simulations of a vertically stratified shearing box, in which the turbulent magnetic field is generated by magneto-rotational instability. The main reason of that difference is based on different microphysics consideration. The stress is assumed to be proportional to the radiation pressure in the  $\alpha$ -prescription, while the stress fluctuations precede pressure fluctuations, or say the magnetic energy fluctuations drive pressure fluctuations in the MHD simulation. However, their MHD simulation focuses on the accretion rate near a fraction of the Eddington limit with normal radiation process rather than neutrino cooling. In our paper we still use the  $\alpha$ -prescription with the large-scale field. Thus we have a thermal unstable conclusion in the radiation-dominated regions of the magnetized disks.

## 5. Disk Outflows and Funnel Flows

So far we study the structure and luminosity of the magnetized disks with an open or closed field configuration constrained in the disk plane. If we define the Alfvén radius  $r_A$  as the point at which the magnetic pressure  $P_B = B_m^2/8\pi$  equals the ram pressure of the accretion material  $\rho v_r^2$ , and the magnetospheric radius  $r_m$  as the point where the magnetic pressure is approximately equal to the total matter pressure  $P_B \simeq P_{\text{matter}} + \rho v_r^2$ , the disk plane will be disrupted near the magnetosphere with  $r \leq r_A$  as shown in equation (1) and Figure 1, and the disk flow will be prevented from accretion in the disk plane at  $r_m$ . Then almost the entire disk will be funneled along the magnetar field lines onto only a small fraction region of the stellar surface at  $r < r_m$ . The value of  $r_m$  depends on the details of disk-magnetar interaction. In the normal case such as accretion onto magnetized neutron stars in X-ray binaries, we have  $P_{\text{matter}} \ll \rho v_r^2$ . Thus  $r_m$  can be calculated as  $P_B \sim \rho v_r^2$ . It is estimated that  $r_m$  is close to or slightly less than the Alfvén radius (Lai 1998). Let us see the situation in the magnetized hyperaccreting disks. Differently we have  $\rho v_r^2 < P_{\text{matter}}$  or  $v_r < c_s$  in the disk plane for the hyperaccreting case. Figure 11 gives the pressure ratio of magnetic stress and matter stress, and the cooling efficiency along the radius. In this Figure we confine the calculation in the disk plane without considering the funnel effect. We find that the pressure ratio keeps  $P_B/P_{\text{matter}} < 1$  in the disk plane, thus the accretion flow can hardly be lifted by the field pressure above the plane. However, since the accretion flow begins to co-

rotate with the magnetar surface inside the Alfvén radius, the viscous heating and angular transport which are generated by differential rotation in the disk become ignorable. Also, the generated azimuthal component of the disk field, which is proportional to the difference between the disk and magnetar surface angular velocity, should also be ignorable. As a result, the disk begins to cool and loss its angular momentum. The matter pressure  $P_{\text{matter}}$  drops at the radius inside the Alfvén radius. In addition, as the magnetic pressure increases as the accretion flow moving towards the magnetar surface, the ratio  $P_{\text{B}}/P_{\text{matter}}$  keeps to increase and can be greater than unity as well. Thus the magnetosphere (with its edge at  $r_m$ ) can actually form inside the Alfvén radius, i.e., we still have the magnetosphere region with  $r_* < r_m < r_A$  in the magnetized hyperaccreting disks.

Furthermore, the strong field in the Alfvén radius would cause a magnetically-driven outflow from the inner disk region; the interaction between the disk and central star is favorable for launching an X-type wind from the disk-magnetosphere boundary (Shu et al. 1994), both of which also decrease the pressure of the accretion matter and increase the ratio  $P_{\text{B}}/P_{\text{matter}}$ . On the contrary, it is most likely that an thermally-driven outflow can form in this outer region  $r > r_A$ . Generally speaking, the thermal outflow can take away angular momentum and energy outside  $r_A$ , make the direct flow accretion rate into the magnetosphere and magnetar surface be low and give a possible energy source for a supernova explosion associated with a GRB.

In Section 5.1, we discuss the disk outflow caused by thermal heating. In Section 5.2 we discuss the funnel flow process due to the co-rotation and magnetic pressure near the stellar magnetosphere.

### 5.1. Disk Outflows

The thermal wind is induced by viscous heating (MacFadyen & Woosley 1999), or neutrino heating (Metzger et al. 2008b), depending on the dominated heating and cooling processes in the disk. In paper II, we study the structure of the neutron star disk outflows around neutron stars without fields. As shown by Narayan & Yi (1994, 1995), if the adiabatic index  $\gamma < 3/2$  in an advection-dominated flow, the Bernoulli constant of the flow is positive and a thermally driven wind can be driven from the disk. In this case, the energy carried by the outflow is expected to feed a supernova explosion, which is associated with a GRB in the collapsar scenario (MacFayden & Woosley 1999; Kohri et al. 2005). This thermally-driven wind can also exist in the magnetized disks beyond the Alfvén radius, where the matter pressure dominates over the magnetic pressure, and heating energy generated by viscous and Joule dissipation is advected inward along the disk radius. As showed in Figure 11 (right

panels), the neutrino cooling efficiency increases with increasing the strength of a magnetic field for  $\dot{M} \sim 0.1M_\odot \text{ s}^{-1}$ , and the entire disk beyond the Alfvén radius becomes neutrino-dominated for  $\dot{M} \sim 1.0M_\odot \text{ s}^{-1}$ . Therefore the outflow-driven process should be significant below  $\dot{M} \sim 1.0M_\odot \text{ s}^{-1}$ . In this section, we adopt the similar treatment as in Kohri et al. (2005) and paper II for simplicity, i.e., we only consider the viscously induced outflows and assume the accretion rate varies as a power law in radius for the case  $\dot{M} < 1.0M_\odot \text{ s}^{-1}$  as

$$\dot{M} = \dot{M}_{\text{out}} \left( \frac{r}{r_{\text{out}}} \right)^\xi, \quad (45)$$

where  $\dot{M}_{\text{out}}$  is the initial accretion rate at the outer edge of the disk, and  $\xi$  is the outflow index in the disk. Stronger outflows have a lower value of  $\xi$ . Using the outflow structure (45), the angular momentum equation (26) is modified as

$$\frac{1}{1 + 2\xi} \frac{\dot{M}}{3\pi} f = \nu\Sigma - \frac{\dot{M}N_B}{3\pi r^2\Omega}. \quad (46)$$

Here we have assumed that the outflow has the same angular velocity as the accretion flow outside the Alfvén radius and takes away angular momentum from the disk.

Figure 12 gives the disk structure with a viscous and Joule heating induced thermally-driven outflow for various outflow index  $\xi = 0.2, 0.6, 0.9$ , different magnetar surface fields  $B_0 = 10^{16}, 10^{17} \text{ G}$ , and a fixed accretion rate  $\dot{M} = 0.5M_\odot \text{ s}^{-1}$  in the radius  $r = 124 \text{ km}$  (i.e.,  $30R_{sh}$  of a  $1.4 M_\odot$  star). Similar to the results in paper II, the density, pressure and neutrino luminosity decrease with increasing the outflow strength. On the other hand, the ratio of  $P_B/P_{\text{matter}}$  and the thickness of the disk become larger for stronger outflows. Therefore a disk with stronger thermally-driven outflow outside the Alfvén radius carries more energy away into the stellar envelope at a fixed radius. However, the total outflow energy strongly depends on the size of the region outside the Alfvén radius, where generates viscous and Joule heating energy and induces outflows. A strong central stellar field makes the Alfvén radius be larger and decrease the total heating and the potential outflow injection energy. Table 1 gives our estimate of the maximum energy carried by the outflow, which can be calculated as the difference between heating energy with and without field,

$$\begin{aligned} \dot{E}_{\text{out,max}} &\sim \int_{r_A}^{r_{\text{out}}} Q_{\text{heat}}^+(\xi = 0) 2\pi r dr - \int_{r_A}^{r_{\text{out}}} Q_{\text{heat}}^+(\xi) 2\pi r dr \\ &= \frac{3GM\dot{M}}{4} \left\{ \frac{1}{3r_A} - \frac{1}{r_{\text{out}}} \left[ 1 - \frac{2}{3} \left( \frac{r_A}{r_{\text{out}}} \right)^{1/2} \right] \right\} \\ &\quad - \int_{r_A}^{r_{\text{out}}} \frac{9}{8} \nu \Sigma \frac{GM}{r^3} 2\pi r dr + [\dot{E}_{\text{joul}}(\xi = 0) - \dot{E}_{\text{joul}}(\xi)] \end{aligned} \quad (47)$$

The maximum energy injection rate decreases significantly for stronger stellar fields, which make the magnetically-driven wind and funnel effect be more important than the thermal outflow for strong fields.

Besides the thermally-driven outflow in the disk outer region, a strong field inside the Alfvén radius causes the accretion flow to co-rotate with the stellar field, and is possible to launch MHD wind along the field lines (Metzger et al. 2008a). Moreover, it is also clear that an X-type field configuration near the central star is favorable for launching magnetically-driven wind from the disk-magnetosphere boundary (Shu et al. 1994). As showed by simulations (e.g., Romanova et al. 2008), the properties of these MHD outflows depend on many factors such as the field structure, the accretion rate, the related viscosity and magnetic diffusivity, etc. The magnetically-driven winds in the disk inner region will decrease the rate of accretion onto the magnetar surface. Also, the magnetically-driven winds can provide energy to a supernova explosion together with the thermal outflow. But this issue is beyond the purpose of this paper.

## 5.2. Funnel Flows from Disks to Magnetars

When the magnetic pressure becomes equal or larger than the matter pressure inside the Alfvén radius  $P_B \geq P_{\text{matter}}$ , the funnel accretion process becomes significant. For the case of hyperaccreting disks, this process can only be important for an extremely strong field, which depends on the accretion rate. For simplicity, we consider the funnel process to take in the region between the magnetosphere and the Alfvén radius, and the accretion in the disk plane will be truncated at the radius  $r_m$ . The scenario of funneling process is similar to many previous work (e.g. Lovelace et al. 1995, Fig 2, Fig 3; Koldoba et al. 2002, Fig 1; Frank et al. 2002, Fig 6.4). Different to the disk with cylindrical coordinates, in this section we use the spherical coordinates  $(r_l, \theta, \phi)$  with origin at the stellar center to describe the funneled flow, where  $\theta$  is the angle between the axis of the disk plane and a given polar radius  $r$ ,  $\phi$  is the angle in the disk plane. Thus the equation for the dipole field geometry line is (Frank et al. 2002)

$$r_l = r_d \frac{\sin^2 \theta}{\sin^2 \Theta}, \quad (48)$$

where  $r_d$  is the radius at which the magnetic field line passes through the disk, and  $\Theta$  is the angle between the magnetic pole and disk axis. We can approximately take  $r_m < r_d < r_A$ .

The magnetic field along the field line reads

$$B_p(r_l) = B_0 \left( \frac{r_*}{r_l} \right)^3 (4 - 3\sin^2 \theta) = B_0 \left( \frac{r_*}{r_l} \right)^3 \left( 4 - \frac{3r_l}{r_d} \sin^2 \Theta \right)^{1/2}. \quad (49)$$

Note that the dipole field is somewhat different to the vertical component  $B_z(r) = B_0(r_*/r)^3$  in Section 3, in which  $r$  is the radius of the disk in the disk plane. The mass conversation along the magnetic flux line requires the poloidal part  $(r, \theta)$  of the velocity  $v_p$  and the density  $\rho$  satisfies

$$\frac{4\pi v_p \rho}{B_p} = K, \quad (50)$$

where  $K$  is the constant along the flux line. Near the magnetar surface, the accretion rate satisfies

$$4\pi r_*^2 v_* \rho_* \left( \frac{\Delta\Omega}{2\pi} \right) = \dot{M}, \quad (51)$$

where  $\Delta\Omega$  is the opening solid angle of the funnel flows,  $v_*$  and  $\rho_*$  is the average velocity and density in this angle  $\Delta\Omega$  onto the stellar surface. We use the  $2\pi$  as the total solid angle because the funnel flow can be accreted towards two poles. The difference between the final accretion rate  $\dot{M}$  onto the magnetar surface and the initial accretion rate  $\dot{M}_{\text{out}}$  in the disk strongly depends on the strength of magnetically and thermally driven winds. Different to the case of Bondi accretion onto a magnetized compact star, which form an accretion column to cover the magnetic pole, the funnel accretion from a half-thickness disk forms a ring-like belt at the latitude of  $\theta$  between  $\arcsin\sqrt{r_*/r_A}$  and  $\arcsin\sqrt{r_*/r_m}$  to cover a part of the stellar surface. Recent simulations show that the geometry shape and physical properties of this belt (or say the “hot spot”) are very complicated, depending on the detailed field topology and the structure of the funnel flows (Long et al. 2008, or see Romanova et al. 2008 for a review). In this paper we take this ring-like belt as axisymmetric around the magnetic pole axis for simplicity. Appendix B gives our estimate of the ratio of  $\Delta\Omega/2\pi$  in the case of hyperaccreting and neutrino-cooled disks. Combining (49), (50) and (51), we have

$$\rho v = \frac{\dot{M}(2\pi/\Delta\Omega)}{4\pi r_*^2} \left( \frac{B_p}{B_{p*}} \right). \quad (52)$$

with  $B_{p*}$  being the strength of the dipole field on the stellar surface.

In the normal cases, the infalling funneled flow from the disk plane onto a magnetized compact star usually will go through a strong shock before reaching the stellar surface (e.g., Ferrari et al. 1985; Ryu et al. 1996; Li et al. 1996; Frank et al. 2002). However, such a shock is probably unlikely to develop in the hyperaccreting disks. Let us discuss it in more details. The Mach number  $\mathcal{M}$  in the funnel flow along the magnetic field pole can be calculated as

$$\mathcal{M}^2 = \frac{v^2}{a^2} = \frac{(v\rho)^2}{\gamma\rho P_{\text{matter}}} = \left( \frac{\dot{M}}{4\pi r_*^2} \right)^2 \left( \frac{2\pi}{\Delta\Omega} \right)^2 \left( \frac{B_p}{B_{p*}} \right)^2 \frac{1}{\gamma\rho P_{\text{matter}}} \quad (53)$$

with  $\gamma$  being the adiabatic index of the disk matter. Thus

$$\begin{aligned} \mathcal{M}^2 &\sim 8\pi \left( \frac{\dot{M}}{4\pi r_*^2} \right)^2 \left( \frac{2\pi}{\Delta\Omega} \right)^2 \left( \frac{B_p}{B_{p*}} \right)^2 \left( \frac{P_B}{P_{\text{matter}}} \right) \frac{1}{\gamma B_p^2 \rho} \\ &= 6.30 \times 10^{-5} \gamma^{-1} \rho_{12}^{-1} \dot{M}_{-1}^2 r_{*,6}^{-4} B_{p*,16}^{-2} (2\pi/\Delta\Omega)^2 (P_B/P_{\text{matter}}), \end{aligned} \quad (54)$$

where  $\rho_{12} = \rho/10^{12} \text{ g cm}^{-3}$  and  $B_{p*,16} = B_{p*}/10^{16} \text{ G}$ . For a typical hyperaccreting disk with a stellar field  $\sim 10^{16} \text{ G}$  and the accretion rate  $\dot{M} = 0.1 M_\odot \text{ s}^{-1}$ , we have  $P_B \sim P_{\text{matter}}$ ,  $\rho \sim 10^{12} \text{ g cm}^{-3}$ , and  $2\pi/\Delta\Omega \sim 10^2$  (from Appendix B), therefore the Mach number is  $\mathcal{M} < 1$ , which shows there is no shock wave existing in the funnel flow. A strong magnetically-driven wind will make the density and pressure in the funnel flow decrease, but the accretion rate  $\dot{M}$  onto the star will also decrease. Although  $2\pi/\Delta\Omega$  can reach to  $10^3$  and the factor  $P_B/P_{\text{matter}}$  increases for a strong field  $\sim 10^{17} \text{ G}$  with  $\dot{M} = 0.1 M_\odot \text{ s}^{-1}$ , but the decreasing factor  $\rho_{12}^{-1} B_{p*,16}^{-2}$  makes the Mach number hardly exceed unity.

In the funnel channel, the flow is accelerated via the stellar gravitational force. The gravitational binding energy is converted to the kinematic energy of the flow, then the kinematic energy will be converted to the heating energy near the magnetar surface, which is cooled via thermal neutrino emission. The total energy release rate in the funnel process can be approximately taken as

$$\dot{E}_{\text{funnel}} \sim \frac{GM\dot{M}}{4} \left( \frac{1}{r_*} - \frac{1}{r_A} \right), \quad (55)$$

and the energy equation in the magnetar surface boundary is

$$\frac{7}{8} \frac{\sigma_B T^4}{\tau_\nu} \cdot S = \frac{GM\dot{M}}{4r_*} \epsilon, \quad (56)$$

where the parameter  $\epsilon$  is introduced to show the combined efficiency of acceleration and cooling. The accretion rate here is adopted as the final accretion rate onto the magnetar. The area of the “hot spot” is  $S = \Delta\Omega r_*^2$ . Here we consider the new born magnetar with a lifetime  $\gg 100 \text{ ms}$  (Dessart et al. 2009), then the temperature of the “hot spot” can be significantly higher than the other region of the magnetar surface. The temperature in the “hot spot” can be calculated as

$$T = 7.4 \times 10^{10} (2\pi M_{1.4} \dot{M}_{-1} \epsilon / \Delta\Omega)^{1/4} r_*^{-3/4} \text{ K}, \quad (57)$$

where we take  $\epsilon$  as 0.5. Since the temperature is insensitive to the neutrino optical depth as  $\tau_\nu^{1/4}$ , we take  $\tau_\nu \sim 1$  in our calculation. The temperature in this surface region increases slightly with increasing the ratio of  $2\pi/\Delta\Omega$ :  $T = 1.3 \times 10^{11} \text{ K}$  (10 MeV) for  $2\pi/\Delta\Omega = 10$ , or  $T = 2.3 \times 10^{11} \text{ K}$  (20 MeV) for  $2\pi/\Delta\Omega = 100$ .

The neutrino pair annihilation process  $\nu_i + \bar{\nu}_i \rightarrow e^- + e^+$  is the most important mechanism to provide the energy for a relativistic jet formed from the neutron star disk with weak stellar magnetic field. According to paper II, the neutron star disk with a hot stellar surface layer could increase the neutrino annihilation luminosity by about one order of magnitude higher compared with the black hole disk. If the stellar field is strong up to  $\geq 10^{15}$  G, as discussed in Section 3, the disk with strong magnetic field will have a higher density, pressure and neutrino luminosity, therefore the annihilation rate above the disk plane will also be higher than that emitted from a disk with the same radius range without field or with weak field. This conclusion is similar to that in Lei et al. (2009, their Fig. 2). However, the strong field truncate the disk plane accreting in the inner region and will decrease the total annihilation luminosity from the disk. In this case, the annihilation mechanism will be more significant from the magnetar surface where accretes the funnel flow. Similar to the case without field, the total neutrino annihilation rate is contributed by three components: the annihilation between neutrinos both from the disk, both from the stellar surface, and one from the disk and the other from the stellar surface respectively. If the stellar surface is bright to neutrino emission, then the stellar surface will contribute to the main annihilation luminosity in the accreting system. This is why the neutron star accretion system will have a brighter annihilation luminosity than its black hole counterpart. In the funnel process, on the other hand, the stellar surface area where has a solid angle  $\Delta\Omega \ll 2\pi$  and higher latitude  $\theta_* \sim \arcsin\sqrt{r_*/r_A}$  to emit thermal neutrino will be more geometrical concentrative and hotter than that without field, so the annihilation rate will be more efficient (Birkel et al. 2007). Figure 13 shows the neutrino annihilation rate as a function of height along the magnetic poles with different latitudes of the emitting “hot spot” area. We adopt the formula of neutrino annihilation as in Popham et al. (1999) and Rosswog et al. (2003). The different point here is that the neutrinosphere is a ring-like belt around the magnetar surface, but not a plane disk. The neutrino annihilation rate  $l_{\nu\bar{\nu}}$  from a higher latitude ring-like belt area is larger near the stellar magnetic poles, but becomes smaller far from the poles. That is because the shorter distance of a given point along the pole to a higher latitude emission area plays a key role in increasing the annihilation efficiency. On the other hand, the less average value of the angle or larger  $\cos\theta_{kk'}$  between neutrino pairs from lower latitudes plays a more important role in increasing the neutrino annihilation efficiency at a large height  $\geq 20$  km. Whatever, the integrated neutrino annihilation energy along the pole region  $\int_{r_*}^{\infty} l_{\nu\bar{\nu}} dz$  is much higher from the higher latitude ring-like belt than that from lower latitudes. Therefore, funnel accretion can accumulate more powerful annihilation luminosity (see the caption of Figure 13).

In the black hole disks with strong fields, the MHD effects such as the Blandford-Znajek mechanism or magnetic instabilities (MRI) leads to formation of a magnetically-dominated

jet along the magnetic poles. Such a magnetically-dominated jet will also form from the magnetar in a few seconds of its formation, and the magnetar rotation energy to feed the jet. Therefore in a hyperaccreting magnetar system the neutrino annihilation mechanism and the MHD mechanism will work together to form a jet, and make the jet be more powerful for a GRB explosion. We will discuss this issue again in Section 6.

Finally we list the properties of the hyperaccreting magnetar system in Table 2, taking the accretion rate  $\dot{M} = 0.1M_{\odot} \text{ s}^{-1}$  near the Alfvén radius  $r_A$  or the stellar surface  $r_*$  (depends on  $r_A > r_*$  or  $r_A < r_*$ ) as an example.

## 6. Discussions

### 6.1. Joule Dissipation

In Section 3 we discuss two competitive sets of effects to affect the disk structure and neutrino emission, i.e., the microphysical quantum effects and the macrophysics magnetic field coupling in the disk MHD equations. The quantum effects decrease the pressure, density and luminosity with increasing the strength of field, but magnetic coupling makes these quantities be higher. However, in most cases, the magnetic field coupling is more important than the quantum effects in a microphysical scale. We discuss this conclusion in details in this section. In fact, in order to see the quantum effects clearly in Figure 4, we adopt a unified field (i.e, without a dipolar form) in the disk, and find that this microphysical effect becomes more significant in the disk region at relatively larger radius. However, such a situation is unreal if we adopt the dipolar field from the stellar surface, thus the microphysical quantum effects will be less important as showed in Figure 4. On the other hand, as showed in the angular momentum equations (35), (37) and the local energy equation (38), (39), stronger magnetic fields will be more important to transfer angular momentum in the disk, as well as to heat the disk by Joule dissipation. Therefore, it is not difficult to understand why the disk with a stronger field will be hotter, denser with higher pressure and brighter neutrino luminosity.

In fact, the parameter  $\beta$  which gives the relation between the vertical and azimuthal components of the disk magnetic field as in equation (32, i.e., the closed field configuration) can be calculated using the Ohm’s law  $\mathbf{j} = \sigma_m(\mathbf{E} + \mathbf{v} \times \mathbf{B})/c$  and Ampere’s law  $\nabla \times \mathbf{B} = 4\pi\mathbf{j}/c$ . We have (Lee 1999)

$$\beta = \frac{4\pi\sigma_m}{c^2} Hr\Omega_K = \frac{Hr\Omega_K}{\eta_m}, \quad (58)$$

where  $\sigma_m$  and  $\eta_m$  are the microscopic electric conductivity and magnetic diffusivity. However,

as argued by some authors (e.g, Bisnovatyi-Kogan & Ruzmaikin 1976; Lovelace et al. 1995; Bisnovatyi-Kogan & Lovelace 1997), since the accretion flow are in general turbulent, the microscopic  $\eta_m$  should be replaced by a turbulent transport parameter  $\eta_t$ , which can be considered as being comparable to the turbulent  $\alpha$  viscosity  $\eta_t \sim \nu \sim \alpha c_s H$ . In this case, equation (58) gives the relation  $\beta \sim v_K \alpha^{-1} c_s^{-1}$ . However, this new relation has its limitations. As discussed by Lovelace et al. (1995), the twist  $|B_\phi/B_z|$  can never be much larger than unity. Therefore, in this paper, we take  $\beta$  as a parameter rather than an obtained variable. Similar to Lai (1998), we consider that  $\beta \sim 1$  as the maximum twist of the original magnetic field from the central stellar surface. On the other hand, we take the magnetic diffusivity  $\eta_t$  in the local energy equation to be the order of the turbulent viscosity. As a result the magnetic diffusivity can be smaller than the classical diffusivity showed by Ghosh & Lamb (1979a, 1979b; see Lovelace et al. 1995 for further discussion).

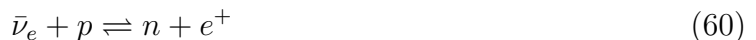
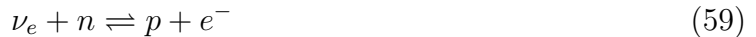
The Joule heating plays a key role in affecting the neutrino luminosity from the hyperaccreting disks with small radius, because the ratio of the viscous heating and Joule dissipation will decrease with small radius, and the Joule dissipation quickly dominates over the viscosity as the main heating source in the disk. Of course all of these results only occur in the region outside the Alfvén radius  $r_A$ , although we usually give our calculations extended to the inner region. Figure 14 shows the neutrino cooling luminosity without Joule dissipation. Compared with the neutrino luminosity from the disk with Joule dissipation in Figures 5, 7, and 9, the main difference is that the neutrino luminosity drops quickly in relatively strong fields at small radius without fields, except for the case that the disk has relatively low accretion rate and is advection-dominated. This result is consistent with the above discussion that Joule dissipation plays a key role in heating the disk inner region near the Alfvén radius.

## 6.2. Application to GRBs

As showed in Section 5.2, the funnel accretion makes the ring-like belt of “hot spot” be more concentrative with higher latitude than the equatorial accretion without fields or with moderate fields. Also, the neutrino luminosity outside the Alfvén radius is also brighter for stronger stellar fields. As a result, the neutrino annihilation efficiency will be significantly increased in the hyperaccreting disks around magnetars compared to the normal neutron star disks, and definitely more efficient than the black hole disks. However, a higher concentration neutrino emission region means higher temperature on the magnetar surface with more massive neutrino-driven winds (Qian & Woosley 1996; Dessart et al. 2009), which will make the jet be heavily baryon-loading. The problem is that, whether the more powerful

annihilation and massive mass loss rate driven by neutrino absorption can work together to produce a relativistic jet required for a GRB explosion? This problem is similar to that in the neutron star disks without fields, which has been discussed in paper II. We consider that a GRB-related jet forms along the stellar poles (i.e., the disk axis if there is no field), and only the wind materials along this axis can feed the jet and affect the bulk Lorentz factor of the jet. The wind ejected in a off-axis direction and that evaporated from the disk will not affect the jet, but only affect the potential supernova explosion associated with the GRB. If there is not disk around the central compact star, the neutrino-driven wind from the star surface can be reasonably approximated as a quasi-steady spherical outflow (Qian & Woosley 1996). However, the hyperaccreting accretion disk around the star can change the distribution of the neutrino-driven wind significantly. The entire stellar surface will be very hot and inject a heavily mass-loading wind along the axis after its formation in a timescale of  $\sim 100$  ms, and then to cool down with the power law  $\dot{M}_{\text{wind}} \propto t^{-5/3}$ . In most cases, the surface ring-like belt region where directly accretes the disk flow will be the hottest region in the disk for the time  $\gg 100$  ms. However, most parts of the wind from this ring-like belt should be off-axis. The polar region that directly drives a wind along the axis is cooler than the equatorial ring-like belt. Even though, we use the temperature of the hot ring-like belt to estimate the maximum strength of the neutrino-driven wind along the poles, and calculate the bulk Lorentz factor of the wind along the pole with field  $\leq 10^{15}$  G in paper II. A moderately or ultra relativistic jet can be produced in the hyperaccreting neutron star system with sufficient high disk accretion rate and bright boundary emission.

However, the situation in a strong field will be different in some aspects. First of all, the neutrino-to-nucleon absorption reaction rate, which is dominated by



will be significantly reduced in strong fields  $B_0 \geq 10^{16}$  G (Duan & Qian 2004, 2005) because of the quantum effects. As a result, the mass loss rate from the stellar surface which is proportional to the absorption rates will decrease as well. Moreover, we have to note that part of the newly generated  $e^-e^+$  particles in the neutrino absorption reaction will move along the closed field lines from the stellar surface rather than be injected far away from the central star. There are some open field lines in the surface region near the stellar magnetic poles (Lovelace et al. 1995), but many of them are more likely to induce winds off-axis rather than the neutrino-driven wind. As a result, the total mass loss rate  $\dot{M}_{\text{polar}}$  along the magnetic polar region will be only a fraction of the total mass loss rate  $\dot{M}_{\text{wind}}$ . On the other hand, the field structure around the stellar surface will also affect the neutrino annihilation process, because part of the generated  $e^-e^+$  pairs in the reaction  $\nu_i + \bar{\nu}_i \rightarrow e^- + e^+$  will also move along

the closed field lines. Therefore, part of the neutrino annihilation energy cannot be loaded into the jet which propagates along the magnetic poles. The precise fraction of the total annihilation energy feeding the polar jet depends on the energy-momentum distribution of the  $e^-e^+$  pairs above the central star and the entire disk, as well as the ratio of  $e^-e^+$  plasma pressure to the magnetic pressure. The reliable estimate of these considerations requires further MHD simulations. However, since the annihilation process happens in the extended space above the accreting system, while the neutrino absorption reaction mainly occurs around the stellar surface with a sufficient high density of nucleons, the strong magnetic fields will play more significant role in changing the properties of the neutrino-driven wind rather than the annihilation process. Therefore the mass loaded in the jet will decrease more significantly than that of the annihilation energy. Based on these above considerations, that is, the neutrino annihilation efficiency is larger for a magnetized disk, such an efficiency can even higher for the funnel accretion process, and the mass loss along the magnetic poles  $\dot{M}_{\text{wind}}$  decreases in strong fields, we can conclude that the jet along the magnetic poles can be accelerated to a larger bulk Lorentz factor compared with its neutron star counterparts without fields or with weak fields. In addition, if the magnetic pole and the disk axis do not overlap ( $\Theta \neq 90^\circ$ ), the direction of the relativistic jet and the disk rotation axis will also not overlap. This is an interesting topic, because if the annihilation rate from the disk is much less than that from the star, the jet will precess along the disk axis with a period of the magnetar.

Furthermore, another significant difference between a magnetar and a non-magnetized neutron star in the hyperaccreting systems is that, a thermally-dominated neutrino-driven wind from the stellar surface may switch to be magnetically-dominated instead after seconds of the compact star formation (Thompson et al. 2004; Metzger et al. 2007). The condition of the magnetic wind can be parameterized using the term of magnetization

$$\sigma = \frac{\Phi_B^2 \Omega_*^2}{\dot{M}_{\text{wind}} c^3} \quad (61)$$

where  $\Phi_B$  is the magnetic flux. The parameter  $\sigma$ , which strongly depends on the rotational period of the central star, is the maximum Lorentz factor the wind can achieve if all magnetic energy is converted into kinetic energy, either via magnetic reconnection (Spruit et al. 2001) or collimation by the interaction between the wind and the the stellar envelope (Bucciantini et al. 2006, 2007, 2009; Tchekhovskoy et al. 2008, 2009). The critical period for  $\sigma \geq 1$ , i.e., the wind to be magnetically-dominated and relativistic is

$$P_{rc} \leq 85 B_{0,16} r_{*,6}^2 \dot{M}_{\text{wind},-5}^{-1/2} \text{ms}. \quad (62)$$

The critical period  $P_{rc}$  increases with increasing the stellar field, and decreases with increasing the mass loss rate  $\dot{M}$ . The properties of the magnetically-dominated wind will be different

with different ranges of  $\sigma$  for the stellar period  $P_r \leq P_{rc}$ . The wind is collimated along the magnetic poles for  $\sigma < 5$ , but will be distributed around the direction at low latitudes and the equatorial plane for  $\sigma > 30$ . For example, Bucciantini et al. (2006, 2007, 2009) showed that, the wind-stellar-envelope interaction may provide a viable mechanism for collimating the jet along the polar region. Their works are based on the consideration that a cavity with the radius  $> 10^8$  cm has been evacuated by the outgoing supernova shock before the compact star formation. Since the wind with high  $\sigma$  is ejected around the equatorial plane initially, whether or not the hyperaccreting disk with a small size  $10^7 - 10^8$  cm can help or prevent the jet collimation needs to be further studied.

It is said that the energy of the magnetically-driven wind is extracted by the central star spin-down process. However, in the magnetar-disk system, if the magnetically-driven wind can be actually collimated along the magnetic polar region, then the stellar spin-down mechanism and neutrino annihilation from the “hot spot” and the entire disk can work together to provide energy of the polar jet and accelerate the jet to an ultra relativistic speed. In this general case, the bulk Lorentz factor can be estimated as

$$\Gamma = \frac{\dot{E}}{\dot{M}_{\text{polar}}c^2}, \quad (63)$$

where the energy feed rate is the summation of neutrino annihilation and the magnetic energy from rotational extraction,

$$\begin{aligned} \dot{E} &= \dot{E}_{\text{anni}} + \dot{E}_{\text{mag}} \\ &= L_{\nu\bar{\nu}}f_k + \dot{E}_{\text{rot}}f_{\text{rot}} = L_{\nu}(f_{\nu\bar{\nu}}f_k) + \dot{E}_{\text{rot}}f_{\text{rot}} \\ &= \frac{GM\dot{M}}{4r_*}(\epsilon f_{\nu\bar{\nu}}f_k) + \frac{2}{5}Mr_*^2\Omega\dot{\Omega}f_{\text{rot}}, \end{aligned} \quad (64)$$

with  $f_{\nu\bar{\nu}}$ ,  $f_k$ ,  $f_{\text{rot}}$  being the neutrino annihilation efficiency  $L_{\nu\bar{\nu}}/L_{\nu}$ , the fraction of the deposited annihilation energy to provide the kinetic energy of the stellar wind, and the ratio of magnetic to total spin-down energy respectively.  $\dot{M}_{\text{polar}}$  as a fraction of  $\dot{M}_{\text{wind}}$  is the wind mass loss rate along the polar region (see paper II for more discussion about the mass loss rate). The ratio of  $\dot{E}_{\text{anni}}$  to  $\dot{E}_{\text{mag}}$  is

$$\frac{\dot{E}_{\text{anni}}}{\dot{E}_{\text{mag}}} = 2.10 \times 10^5 \dot{M}_{-1} P_r^2 \tau_J r_{*,6}^3 \left( \frac{\epsilon f_{\nu\bar{\nu}} f_k}{f_{\text{rot}}} \right), \quad (65)$$

where  $\tau_J$  being the typical spin-down timescale. Based on the analysis in this paper, we take  $\epsilon = 0.5$ ,  $f_{\nu\bar{\nu}} \sim 0.005 - 0.01$  for  $\dot{M}_{-1} \sim 1$ ,  $f_k \sim f_{\text{rot}}$ , and  $\tau_J \sim 7.6 B_{0,16}^{-2} (P_r/1\text{ms})^2 \text{ s}$ ,<sup>4</sup> then the

---

<sup>4</sup>The annihilation efficiency  $f_{\nu\bar{\nu}}$  for a black hole hyperaccreting disk is  $\sim 10^{-4}$  for  $\dot{M} = 0.1M_{\odot} \text{ s}^{-1}$ , and

critical value of the period  $P$  for the ratio  $\dot{E}_{\text{anni}}/\dot{E}_{\text{mag}}$  being less than unity is roughly  $P_r \leq 4$  ms. The critical value  $\sim 4$  ms will even decrease if the disk accretion rate is higher with a higher annihilation efficiency  $f_{\nu\bar{\nu}}$ , or the spin-down timescale is longer. Keep in mind that this critical value is less than  $P_{rc}$  in equation (62), which shows the wind to be magnetically-dominated and relativistic without neutrino annihilation. Therefore, in the extreme case of a millisecond magnetar, the magnetically-dominated jet extracts the rotation energy as the main energy source. If the stellar spin period is around tens to hundreds of milliseconds, the polar jet can be feeded by neutrino annihilation and magnetic energy together, and has a bulk Lorentz factor even higher than  $\sigma$ . On the other hand, for the magnetar period  $P_r \geq P_{rc}$  in equation (62),<sup>5</sup> the jet formation process goes back to be thermally-driven and feeded by the annihilation process as discussed in paper II.<sup>6</sup>

### 6.3. Disk Nucleosynthesis and $r$ -Process Nucleosynthesis

Besides the GRB or GRB-like (e.g., X-ray flashes) phenomena with their associated supernovae, the hyperaccreting magnetar system can also generate enough  $^{56}\text{Ni}$  and other elements from the disk for the supernova (MacFadyen & Woosley 1999; Kohri et al. 2005; Nagataki 2006, 2007), and produce more heavier elements in the neutrino-driven wind via  $r$ -process nucleosynthesis.

Simulation works based on the collapsar scenario (MacFayden & Woosley 1999; Nagataki et al. 2006, 2007) showed that  $^{56}\text{Ni}$  produced in a jet of the collapsar is not sufficient to explain the observed amount in a supernova with a duration about  $\sim 10$  s (e.g., Mazzali et al.

---

this efficiency can be higher and up to  $\sim 10^{-3}$  for the neutron star disk without fields. The value of  $f_{\nu\bar{\nu}}$  can be even higher for a magnetized disk and funnel accretion as mentioned above. We take  $f_{\nu\bar{\nu}} \sim 0.005 - 0.01$ . However, the  $f_{\nu\bar{\nu}}$  value is insensitive to the final results, since the period  $P_r \propto f_{\nu\bar{\nu}}^{-1/4}$ . The spin-down timescale can be approximately taken as the one in Thompson et al. (2004) and Metzger et al. (2007), i.e.,  $\tau_J \propto (P_r/B_0)^2$  for  $r_A < c/\Omega$ .

<sup>5</sup>The maximum initial spin period of newborn pulsars is still under debate. For example, Spruit & Phinney (1998) considered that the newborn pulsar without “kicks” can reach a long initial period  $\sim 100$  s. However, Heger et al. (2005) showed that the spin period of the pulsar formed a the  $10 - 15M_\odot$  star is  $10 - 15$  ms based on their stellar evolution code.

<sup>6</sup>We mention that Harikae et al. (2009) have discussed the combination effects of MHD mechanism and annihilation process in the accreting black hole system based on the collapsar scenario. They showed that the collapsar with an initial field  $\sim 10^{10}$  G and angular momentum of 1.5 times the angular momentum of the last stable orbit can finally produce the MHD outflows and obtain the strong neutrino heating in the polar funnel at the same time. However, how the collapsar can generate a initial field with  $\sim 10^{10}$  G remains an open question.

2006; Soderberg et al. 2008). As a result, the majority of  $^{56}\text{Ni}$  with mass  $\sim 10^{-2}M_{\odot}$  might be synthesized in the accretion disk or in the disk outflows. Nagataki et al. (2007) calculated that the  $^{56}\text{Ni}$  synthesized in the disk can reach  $\sim 10^{-3}M_{\odot}$ , but it should be carried out by a later phase outflow or the viscous induced outflow. Also, Kohri et al. (2005) discussed that the recombination process of nucleons ( $n, p$ ) into nuclei can happen in the outflow and release an energy about 8 MeV per nucleon. In the hyperaccreting magnetar scenario, on the other hand, since the disk becomes hotter, denser with higher pressure with a stronger field, the ejected  $^{56}\text{Ni}$  via the disk outflow should be more than that estimated in the some region of the collapsar without fields. However, if the magnetar field strength is high enough and the funnel accretion is obvious, the disk region outside the Alfvén radius  $r_A$  will be relatively small and ejected even less  $^{56}\text{Ni}$ . Also, in the co-rotation region without viscous heating at radius less than  $r_A$ , the disk will be cooled down and produce much less  $^{56}\text{Ni}$ .

The main properties to determine the  $r$ -process production are the asymptotic wind entropy  $S^a$ , asymptotic electron fraction  $Y_e^a$  and dynamical timescale  $t_{\text{dyn}}$ . In general, higher wind entropy, lower electron fraction and short dynamical timescale are more favorable to produce heavier nuclei with higher maximum  $A$  number (Meyer & Brown 1997; see also Thompson 2003). Although the winds are thought to be a candidate for the  $r$ -process, recent models without fields showed that the winds are difficult to produce robust  $r$ -process nucleosynthesis for the “classical” neutron star with a  $1.4M_{\odot}$  mass and 10 km radius (e.g., Qian & Woosley 1996; Thompson et al. 2001). Thompson (2003) roughly estimated the  $r$ -process in the strong field environment with  $B_0 \geq 6 \times 10^{14}$  G. Since the strong field can trap the wind in the neutrino heating region, the amplification of the trapping timescale can lead to the amplification of the entropy. This amplification may be sufficient to yield robust third-peak  $r$ -process nucleosynthesis. In addition, Metzger et al. (2007) showed that the presence of a magnetar field  $\sim 2 \times 10^{14}$  G and mildly rapid rotation  $\sim 10$  ms moves the ratio  $(S^a)^3/t_{\text{dyn}}$ , which is the critical wind parameter to determine the condition for an  $r$ -process, an order of magnitude more favorable for third-peak  $r$ -process nucleosynthesis. Therefore, the magnetic fields from the central magnetar may play significant role in inducing a successful strong  $r$ -process nucleosynthesis. However, the problem is that, all of the works considering magnetic fields do not include the strong field quantum effects on the state of equations of the wind. In other words, they do not consider the Landau level effect and the neutrino absorption reaction rate modified by the strong fields. As discussed in Section 6.2, the strong field can decrease the neutrino absorption reaction rate, and also decrease the mass loss rate of the neutrino-driven wind as well. Also, the strong field can affect the density and pressure distribution in the wind. Therefore, it is interesting to consider whether the microphysical change in the strong field can affect the final results of the  $r$ -process nucleosynthesis. Furthermore, if we look into the scenario of hyperaccreting disks,

we should keep in mind that the disk will increase the wind entropy and affect its distribution in the polar region where propagates the stellar neutrino-driven wind (e.g., Nagataki et al. 2006, 2007). Another possibility is that the disk outflows and the X-type winds, rather than the stellar neutrino-driven winds, will also produce the  $r$ -process elements with  $A > 130$ , because the neutrino-to-proton ratio in the disk and the outflows are sufficiently high, and the mass loss rate from the disk is much higher than that from the stellar surface (Kohri et al. 2005). However, whether the disk outflows can be the site for  $r$ -process nucleosynthesis is still under debate (Metzger et al. 2008a). Since the pressure of the outflow will drop quickly above the disk and be less than the magnetic pressure, the magnetic field above the disk may also play significant role in increasing the outflow entropy as discussed in Thompson (2003). As a result, more work should be done to understand the influence of a strong field on the  $r$ -process in the hyperaccreting magnetar systems.

#### 6.4. A Unified Scenario of Collapse-related-GRB Models

Let us compare the hyperaccreting neutron star/magnetar model with the isolated magnetar model, both of which are proposed to be able to produce GRB and GRB-like events. The hyperaccreting neutron star/magnetar disks can form in collapsars or compact binary mergers. In the collapsar scenario, rotation and magnetic fields make the core be possible to collapse into a massive neutron star/magnetar rather than a black hole. On the other hand, isolated magnetars are proposed to form via the rotating Type-Ib/c supernovae, the mergers of compact binaries, or the accretion-induced collapse of white dwarfs. Therefore, the progenitors of the hyperaccreting compact star model and the isolated magnetar model are actually very similar with each other. The main difference is the environment: the disk around the neutron star/magnetar will produce significant phenomena which will not be produced by the isolated magnetar. Let us see the case of massive star collapse for example. The isolated magnetar forms after a successful supernova explosion, and the supernova shock has created a cavity around the magnetar before it drives magnetically-dominated and Poynting-dominated winds. On the contrary, the unsuccessful or weak ongoing shock leads to the hyperaccreting system. The disk material around the neutron star/magnetar comes from the continuous infalling stellar envelope, or the fallback of stellar material which has been ejected by the shock but cannot reach sufficiently high velocity to escape the gravitational potential of the core. Kumar et al. (2008) discussed the accretion rate of different accretion stages, in which the accretion rate is different depending on which stellar zone is accreted.

We try to use a unified point of view to consider the outcomes of the massive star

collapse. If the core collapse can initiate a successful supernova, then an isolated black hole or a rotating magnetar can form in the supernova remnant. Vietri & Stella (1998, 1999) discussed the possibility of a neutron star further losing its angular momentum by magnetic dipole or gravitational waves radiation during a long time and collapsing to an accreting black hole. In addition, the magnetar model shows the possibility that a variety of magnetic activities from the isolate magnetar can produce a GRB explosion after the supernova for a short time. On the other hand, if the outgoing shock formed during a core collapse cannot compete the continuous accretion from the stellar envelope, the collapse leads to the formation of a collapsar system, in which the type of the central compact object depends on many factors such as rotation, equations of state and so on. The black hole disk may produce a GRB explosion via neutrino annihilation or MHD processes, but the annihilation mechanism may not produce sufficient energy for energetic GRBs. The neutron star disk will increase the annihilation efficiency compared to its black hole counterpart, and the increased efficiency will be even higher if the central star is a magnetar. In the hyperaccreting magnetar system, the increased annihilation process and the magnetically-driven pulsar wind can work together to generate a more powerful jet than that generated by a single mechanism. The outflows and magnetically-dominated winds from the disk is possible to feed a late-disk-induced supernova associated with the GRB. In a word, the unified scenario shows that the outcomes have a closed relation to the initial stellar properties and the core collapse process itself.

However, such a unified scenario as the GRB central engine candidate cannot be confirmed directly. What we can observe is the GRB-related properties such as photon lightcurve, spectrum, neutrino emission, different bands of afterglows, which can be traced back to the central engine and show evidence for the existence of a central neutron star. We do not want to show further evidences here (see Dai 2004, Dai et al. 2006; Fan & Xu 2006; Yu & Dai 2007 for more details). Finally we want to mention two points. One is that, the intermediate case, i.e., the fallback material forms a normal disk around a magnetar, has been discovered (Wang et al. 2006). Although the disk radiated IR emission is very different to the hyperaccreting disk, this discovery shows a link between isolate magnetar and hyperaccreting magnetar in the core collapses. Another point is that, since some stars that are less massive than Wolf-Rayet stars are more likely to form neutron stars and magnetars, we cannot preclude the possibility that the collapse of stars with an intermediate mass can also lead to the hyperaccreting neutron star/magnetar systems and produce the GRB-like phenomena. In fact, some evidences show that the GRB may be associated with Type II supernova (Germany et al., 2000; Rigon et al., 2003), although the evidences are still controversial today.

## 7. Conclusions

The hyperaccreting neutron star or magnetar disk systems cooled via neutrino emission can form by the mergers of compact star binaries or the collapses of rotational massive stars. Strong fields of the magnetar can play a significant role in affecting the disk properties and even changing the accretion process. Our motivation in this paper is to investigate the influence of such strong magnetic fields on the disks, and discuss implications of the magnetar disk systems for the GRB and GRB-like events. Our conclusions are as follows.

(i) We consider the magnetar field has a dipolar vertical component  $B_z$ . The differential rotation between the disk and the magnetar will generate a toroidal field component  $B_\phi$ , as well as a relatively weak radial component  $B_r$ . The generated field can have an open or closed configuration, depending on the disk’s viscous turbulence, magnetic diffusivity, disk angular velocity as well as twist limitation. Similar to pervious works, we use the parameter  $\beta$  to measure the strength of the toroidal field (equations (31) and (32)). The generated large-scale disk field coupled with the accretion flows will transfer the angular momentum in radial direction and heat the disk via Joule dissipation together with viscous stress outside the Alfvén radius  $r_A$ . On the other hand, since the distribution and energy of electrons change significantly in the strong field environment, the disk pressure and a variety of neutrino cooling processes will be different compared to the case without fields. Therefore, we discuss the quantum effects of the strong fields on the disk thermodynamic and microphysical processes in Section 2, and list the MHD conservation equations to describe the behavior of the large-scale magnetic field coupling in the disk in Section 3.

(ii) The quantum effects and field coupling in MHD equations play two competitive roles in changing the disk properties, the former to decrease the pressure, density and neutrino luminosity with increasing field strength (Figure 4), while the latter to increase them (Figure 5). However, in most cases the large-scale field coupling is more significant than the microphysical quantum effect (Figure 7). Moreover, strong fields will change the electron fraction distribution  $Y_e$  in the disk significantly. Larger peak of electron chemical potential  $\eta_e$  with more degeneracy electron states is obtained by stronger fields, while the change of  $\eta_e$  becomes more obvious for stronger fields.

(iii) Similar to the neutron star disk without fields, the values of density, pressure, temperature, neutrino luminosity and electron chemical potential become higher for higher accretion rate, but the electron fraction  $Y_e$  decreases with increasing the accretion rate.

(iv) The magnetized disk maintaining a plane geometry would be more favorable for an open field configuration rather than a closed one. However, we still consider the two cases for completeness (Figures 6 and 9). For the disk with an open field and  $\dot{M} = 0.1M_\odot$

$s^{-1}$ , higher ratio of  $\beta/s$  leads to higher density and pressure in the entire disk plane, higher temperature and neutrino luminosity in the inner part of the disk, as well as lower  $Y_e$  in the outer part. Here  $s$  is the ratio of disk angular velocity and the Keplerian velocity. Also, electrons becomes more degeneracy at  $\sim 20 - 40$  km for higher  $\beta/s$ . On the other hand, the disk properties with a closed field not only depends on the values of  $\beta$  and  $s$ , but also the spin period of the central magnetar. Shorter period of the central star decreases the disk density, pressure,  $\eta_e$ , but increases  $Y_e$  at the outer part of the disk. The effects of spin period are only obvious for sufficient field strength (e.g.,  $\sim 10^{16}$  G for the accretion rate  $0.1M_\odot \text{ s}^{-1}$ ) from the central star.

(v) The accretion flow in the disk plane outside the Alfvén radius is viscously stable. However, whether the disk is thermally stable depends on many factors such as the disk region, magnetic field strength, disk angular velocity and accretion rate. Generally speaking, the disk will be definitely thermally unstable if its non-field disk counterpart with the same accretion rate is unstable. The disk region can also be thermally unstable even its non-field counterpart is stable, if the region is near the Alfvén radius where magnetic field plays a more important role in transferring the angular momentum and heating the disk than the viscous stress.

(vi) The thermally-driven outflows can also exist in the magnetar disk beyond the Alfvén radius for the case of  $\dot{M} < 1.0M_\odot \text{ s}^{-1}$ . We assume the accretion rate as a power law in radius for simplicity (Equation (45)). The outflow will take away the disk angular momentum (Equation (46)) and may provide energy for a supernova associated with the GRB explosion. The disk density, pressure and neutrino luminosity decrease with increasing the outflow strength. Also, the ratio of magnetic and matter pressure  $P_B/P_{\text{matter}}$  and the thickness of the disk become larger for stronger outflows. However, since the total energy taken by the thermal outflow depends on the size of the disk plane outside the Alfvén radius, the total energy injection rate from the outflow decreases significantly for stronger stellar fields (Table 1). Besides the thermally-driven outflow, strong fields inside the Alfvén radius lead the accretion flow to co-rotating with the stellar field, which is possible to launch MHD winds along the field lines, and generate the X-type wind near the disk-magnetosphere boundary. These magnetically-dominated winds are nonrelativistic and may provide energy for a supernova explosion.

(vii) In the hyperaccreting disks, the funnel accretion can only be important for extremely strong fields, which depend on the accretion rate. The accretion process along the disk plane will be truncated in the stellar magnetosphere, so most of the accretion flow can be approximately considered as being lifted along the closed field lines onto the magnetar surface. In most cases, the hyperaccreting infalling funnel flow is unlikely to develop a shock

with Mach number greater than unity (equation (54)). The flow is accelerated by the gravitational force and transfers the gravitational binding energy to the kinematic energy and next to the heating energy near the magnetar surface. The funnel flow will cover a ring-like belt of “hot spot” around the magnetar surface and emit thermal neutrinos. Because the temperature is higher and neutrino emission region is more concentrated than the hyper-accreting neutron star without fields, the funnel accretion can accumulate more powerful neutrino annihilation luminosity (Figure 13).

(viii) The neutrino annihilation process both from the magnetar surface and from the disk plane will be higher than that without fields. Moreover, the neutrino annihilation mechanism and the magnetic activity from the stellar surface (i.e., the pulsar wind mechanism) can work together to generate and feed an ultra-relativistic jet along the stellar magnetic poles. If the stellar spin period is sufficiently short (e.g.,  $\sim 4$  ms for the field  $\sim 10^{16}$  G and  $\dot{M} = 0.1M_{\odot} \text{ s}^{-1}$ ), the jet from the magnetar will be magnetically-dominated and mainly feeded by extraction the stellar rotational energy. If the magnetar spin period is long (i.e., longer than the critical value  $P_{rc}$  in Equation (62)), the jet is thermally-driven and feeded by the annihilation process. In the intermediate case, on the other hand, the relativistic jet can be launched by the pulsar-wind-like process and neutrino annihilation together.

## Acknowledgements

We would like to thank the anonymous referee for his/her very useful comments that have allowed us to improve our paper. We also thank Bing Zhang, Todd Thompson and Yi Xie for the helpful discussions and for a critical reading of the text. D.Z. is supported by a Distinguished University Fellowship from the Ohio State University. Z.G.D. is supported by the National Natural Science Foundation of China (grant 10873009) and the National Basic Research Program of China (973 program) No. 2007CB815404.

## A. Disk Equations without Field

The thermodynamical, microphysical and conservation equations in a hyperaccreting disk without fields can be seen in many previous works. In order to compare them with the case with strong fields, we list them systematically in this appendix. Here we do not consider equations of the neutron star inner disk with a self-similar structure as discussed in paper I and paper II.

The electron/positron density number reads

$$n_{e^\pm} = \frac{(m_e c)^3}{\pi^2 \hbar^3} \int_0^\infty \frac{x^2 dx}{e^{(m_e c^2 \sqrt{x^2+1} \mp \mu_e)/k_B T} + 1}, \quad (\text{A1})$$

and the electron/positron pressure is

$$P_{e^\pm} = \frac{1}{3} \frac{m_e^4 c^5}{\pi^2 \hbar^3} \int_0^\infty \frac{x^4}{\sqrt{x^2+1}} \frac{dx}{e^{(m_e c^2 \sqrt{x^2+1} \mp \mu_e)/k_B T} + 1}. \quad (\text{A2})$$

The total pressure is the summation of the pressure of electrons, nucleons, radiation and neutrinos (without magnetic pressure):

$$P = P_{e^-} + P_{e^+} + P_{\text{nuc}} + P_{\text{rad}} + P_\nu, \quad (\text{A3})$$

where  $P_{\text{nuc}} = \rho R T$  and  $P_{\text{rad}} = a_B T^4/3$  with  $R$  being the gas constant and  $a_B$  being the radiation constant.

The total neutrino cooling rate is the same as equation (9) with various absorption and scattering depths showed in the beginning of Section 2.2.

The neutrino cooling by electron-positron captures by nucleons are contributed by three terms as follows:

$$\dot{q}_{p+e^- \rightarrow n+\nu_e} = \tilde{K} n_p \int_q^\infty \varepsilon (\varepsilon^2 - 1)^{1/2} (\varepsilon - q)^3 f_{e^-} d\varepsilon, \quad (\text{A4})$$

$$\dot{q}_{n+e^+ \rightarrow p+\bar{\nu}_e} = \tilde{K} n_n \int_1^\infty \varepsilon (\varepsilon^2 - 1)^{1/2} (\varepsilon + q)^3 f_{e^+} d\varepsilon, \quad (\text{A5})$$

$$\dot{q}_{n \rightarrow p+e^-+\bar{\nu}_e} = \tilde{K} n_n \int_1^q \varepsilon (\varepsilon^2 - 1)^{1/2} (q - \varepsilon)^3 (1 - f_{e^-}) d\varepsilon, \quad (\text{A6})$$

when the field is absent or can be ignored. Here  $\tilde{K}$ ,  $\varepsilon$ ,  $q$  and  $f_{e^\mp}$  as in Equations (11) to (13) in Section 2.2. Other cooling rates without fields have been showed in Section 2.2.

The chemical equilibrium is

$$\ln \left( \frac{n_n}{n_p} \right) = f(\tau_\nu) \frac{2\mu_e - Q}{k_B T} + [1 - f(\tau_\nu)] \frac{\mu_e - Q}{k_B T}, \quad (\text{A7})$$

where the weight factor  $f(\tau_\nu) = \exp(-\tau_\nu)$  combines the formula from the neutrino-transparent limit case with the neutrino-opaque limit case of the  $\beta$ -equilibrium distribution, and  $Q = q m_e c^2$ .

A set of conservation equations without fields are as follows:

Mass conservation (continuity) equation reads

$$\dot{M} = -2\pi r \Sigma v_r, \quad (\text{A8})$$

this equation keeps the same with and without fields in the vertically-integrated disks. However, we should consider another continuity equation for outflows and winds as

$$\dot{M} = -4\pi r^2 \rho v_r (\Delta\Omega/\Omega), \quad (\text{A9})$$

where  $\Delta\Omega$  is the opening solid angle of the wind.

The integrated angular momentum conservation equation is

$$\frac{\dot{M}}{3\pi} f = \nu \Sigma, \quad (\text{A10})$$

The local energy conservation without fields is

$$Q_{\text{vis}}^+ = Q_{\text{adv}}^- + Q_{\nu}^-, \quad (\text{A11})$$

where the viscosity heating term is

$$Q^+ = \frac{3GM\dot{M}}{8\pi r^3} f \quad (\text{A12})$$

and the advection term is

$$Q_{\text{adv}}^- = v_r T \frac{\Sigma}{2r} \left[ \frac{R}{2} (1 + Y_e) + \frac{4}{3} g_* \frac{aT^3}{\rho} \right], \quad (\text{A13})$$

with  $g_* = 2$  for photons and  $g_* = 11/2$  for a plasma of photons and relativistic  $e^-e^+$  pairs.

The charge conservation equation is

$$\frac{\rho Y_e}{m_B} = n_p = n_{e^-} - n_{e^+}, \quad (\text{A14})$$

which will not be changed in strong fields if we do not consider other charged particles created in the strong field environment.

## B. Solid Angle of Funnel Flow

We take two methods to estimate the latitude and area of the ring-like belt of the “hot spot” on the magnetar surface. The first one is just to follow the approximation made in

Section 5.2. We assume that the funnel accretion flow is lifted in the region with radius between  $r_m$  and  $r_A$ , and the disk plane will be truncated at the magnetosphere  $r_m$ . Taking  $r_m = r_A - \delta$ , we have the field line equation from the two disk radius  $r_A$  and  $r_m$  as

$$r_{l1} = r_A \frac{\sin^2 \theta}{\sin^2 \Theta}, \quad (\text{B1})$$

$$r_{l2} = (r_A - \delta) \frac{\sin^2 \theta}{\sin^2 \Theta}, \quad (\text{B2})$$

or we obtain

$$\sin \theta_1 = \left( \frac{r_*}{r_A} \right)^{1/2} \sin \Theta, \quad (\text{B3})$$

$$\sin \theta_2 = \sin(\theta_1 + \Delta\theta) = \left( \frac{r_*}{r_A - \delta} \right)^{1/2} \sin \Theta, \quad (\text{B4})$$

If  $\delta \ll r_A$ ,  $\sin \Theta \simeq 1$ , we can obtain an analytic solution of  $\Delta\theta$  and  $\Delta\Omega/2\pi$ . We have

$$\sin \theta_2 = \sin \theta_1 + \cos \theta_1 \Delta\theta = \left( \frac{r_*}{r_A} \right)^{1/2} \left( 1 + \frac{\delta}{2r_A} \right), \quad (\text{B5})$$

or

$$\Delta\theta = \frac{\delta}{2} \frac{1}{\sqrt{r_A(r_A - r_*)}}, \quad (\text{B6})$$

The solid angle spanned by the hot spot ring-like belt can be calculated as

$$\Delta\Omega = \int_0^{2\pi} d\phi \int_{\theta_1}^{\theta_2} \sin \theta d\theta \quad (\text{B7})$$

and we obtain an analytic result of the ratio  $\Delta\Omega/2\pi$  as a function of  $r_A$  and  $\delta$ .

$$\frac{\Delta\Omega}{2\pi} = \frac{2\pi \sin \theta_1 \Delta\theta}{2\pi} = \frac{\delta}{2r_A} \sqrt{\frac{r_*}{r_A - r_*}}, \quad (\text{B8})$$

We do not want to solve detailed conservation equations or a set of MHD differential equations as in Ustyugova et al. (1999). Table 3 gives the results with different parameters of  $r_A/r_*$ ,  $\delta/r_*$  and  $\Theta$  as in the case of hyperaccreting disks with strong fields. The typical value for  $\Delta\Omega/2\pi$  is around  $10^{-2}$ , except for the case when  $r_A$  is small and  $\delta \sim r_A$ , which can still be considered as disk plane accretion. Stronger field makes the funnel flow be more significant and the value  $\Delta\Omega/2\pi$  be smaller.

Next we give another scenario based on the consideration that the disk has a thickness near the magnetosphere  $r_m$ . We try to give a simple mathematical model: The ring-like belt is formed by the accretion matter at  $r_m$  with different height  $z$  in the vertical direction. In

other words, the ring-like belt area on the magnetar surface can be traced back to the disk plane vertical section at  $r_m$ .

$$r_{l1} = r_m \frac{\sin^2 \theta}{\sin^2 \Theta}, \quad (\text{B9})$$

$$r_{l2} = r' \frac{\sin^2 \theta}{\sin^2 \Theta}, \quad (\text{B10})$$

where  $r'$  satisfies

$$r' = \frac{r_m(1 + H^2/r_m^2)^{1/2}}{\cos^2(H/r_m)} \sin^2 \Theta, \quad (\text{B11})$$

Similarly, if  $\sin \Theta \simeq 1$  and  $H^2/r_m^2 \ll 1$ , we have

$$\sin \theta_1 = \left( \frac{r_*}{r_m} \right)^{1/2} \sin \Theta, \quad (\text{B12})$$

$$\sin \theta_2 = \left( \frac{r_*}{r_m} \right)^{1/2} \frac{\cos(H/r_m)}{(1 + H^2/r_m^2)^{1/4}} \sin \Theta, \quad (\text{B13})$$

$$\Delta \theta = \frac{3}{4} \sqrt{\frac{r_*}{r_m - r_*}} \left( \frac{H}{r_m} \right)^2, \quad (\text{B14})$$

$$\frac{\Delta \Omega}{2\pi} = \frac{2\pi \sin \theta_1 \Delta \theta}{2\pi} = \frac{3}{4} \sqrt{\frac{r_*}{r_m}} \sqrt{\frac{r_*}{r_m - r_*}} \left( \frac{H}{r_m} \right)^2 \quad (\text{B15})$$

We can take  $r_m$  as a fraction of  $r_A$ . Table 4 gives numerical results in this case. The typical value of  $\Delta \Omega/2\pi$  is as  $\sim 10^{-3} - 10^{-2}$ , which can be slightly smaller than that obtained using the first estimation.

On the other hand, the accretion rate onto the neutron star without fields, as discussed in paper II, can be estimated as  $(2\pi r_* H)/(2\pi r_*^2) = H/r_*$  (note that we consider the disk over a half thickness). Thus the solid angle in this case is in the order of  $\geq 0.1$ , which is larger than the area formed by funnel accretion.

## REFERENCES

- Asano, K., & Fukuyama, T. 2000, ApJ, 531, 949  
 Asano, K., & Fukuyama, T. 2001, ApJ, 546, 1019  
 Baiko, D. A., & Yakovlev, D. G. 1999, A&A, 342, 192  
 Balbus, S. A., & Hawley, J. F. 1991, ApJ, 376, 214

- Bezchastnov, V. G., & Haensel, P. 1996, *Phys. Rev. D.*, 54, 3706
- Birkl, R., Aloy, M. A., Janka, H.-T., & Müller, E. 2007, *A&A*, 463, 51
- Bisnovatyi-Kogan, G. S., & Lovelace, R. V. E. 1997, *ApJ*, 486, 43
- Bisnovatyi-Kogan, G. S., & Ruzmaikin, A. A. 1976, *Ap&SS*, 42, 401
- Blandford, R. D., & Znajek, R. L. 1977, *MNRAS*, 179, 433
- Bucciantini, N. et al. 2006, *MNRAS*, 368, 1717
- Bucciantini, N., Quataert, E., et al. 2007, *MNRAS*, 380, 1541
- Bucciantini, N. et al. 2009, *MNRAS*, 396, 2038
- Burrows, A., & Thompson, T. A. 2004, in *Stellar Collapse*, ed. C. L. Fryer ( Dordrecht: Kluwer), 133
- Chen, H.-H., Ruderman, M. A., & Canuto, V. 1974, *Ap&SS*, 31, 187
- Dai, Z. G. 2004, *ApJ*, 606, 1000
- Dai, Z. G., & Lu, T. 1998a, *A&A*, 333, L87
- Dai, Z. G., & Lu, T. 1998b, *Phys. Rev. Lett.*, 81, 4301
- Dai, Z. G., Lu, T., & Peng, Q. H. 1993, *A&A*, 272, 705
- Dai, Z. G., Wang, X. Y., Wu, X. F., & Zhang, B. 2006, *Science*, 311, 1127
- Dessat, L. et al. 2009, *ApJ*, 690, 1681
- Di Matteo, D., Perna, R., & Narayan, R. 2002, *ApJ*, 579, 706
- Dorofeev, O.F., Rodionov V. N. & Ternov I. M. 1985, *Sov. Astron. Lett.*, 11, 123
- Duan, H., & Qian, Y.-Z. 2004, *Phys. Rev. D.*, 69, 123004
- Duan, H., & Qian, Y.-Z. 2005, *Phys. Rev. D.*, 72, 023005
- Duncan, R. C., & Thompson, C. 1992, *ApJ*, 392, 9L
- Eichler, D., Livio, M., Piran, T., & Schramm, D. N. 1989, *Nature*, 340, 126
- Frank, J., King, A., & Raine, D. 2002, *Accretion Power in Astrophysics* (Cambridge: Cambridge Univ. Press)

- Fan, Y. Z., & Xu, D. 2006, MNRAS, 372, L19
- Ferrari, A. et al. 1985, ApJ, 294, 397
- Germany, L. M., et al. 2000, ApJ, 533, 320
- Ghosh, P., & Lamb, F. K. 1978, ApJ, 223, 83
- Ghosh, P., & Lamb, F. K. 1979a, ApJ, 232, 259
- Ghosh, P., & Lamb, F. K. 1979b, ApJ, 234, 296
- Gu, W.-M., Liu, T., & Lu, J.-F. 2006, ApJ, 643, L87
- Hardy, S. J., & Thoma, M. H. 2000, Phys. Rev. D., 63, 025014
- Harikae, S., Takiwaki T., & Kotake, K. 2009, ApJ, 704, 354
- Hayashi, M. R., Shibata, K., & Matsumoto, R. 1996, ApJ, 468, 37
- Heger, A., Woosley, S. E., & Spruit, H. C. 2005, ApJ, 626, 350
- Hirose, S., Blaes, O., & Krolik, J. H. 2009, ApJ, 704, 781
- Janiuk, A. et al. 2004, MNRAS, 355, 950
- Janiuk, A. et al. 2007, ApJ, 664, 1011
- Janiuk, A., & Yuan, Y.-F. 2009, arXiv:0911.0395
- Johnson, M. H., & Lippmann, B. A. Phys. Rev. 1949, 76, 828
- Kaminker, A. D., et al. 1992, Phys. Rev. D., 46, 4133
- Kawanaka, N., & Mineshige, S. 2007, ApJ, 662, 1156
- Kluźniak, W., & Ruderman, M. 1998, ApJ, 505, L113
- Kohri, K., & Mineshige, S. 2002, ApJ, 577, 311
- Kohri, K., Narayan, R., & Piran, T. 2005, ApJ, 629, 341
- Koldoba, A. V. et al. 2002, AJ, 123, 2019
- Königl, A. 1991, ApJ, 370, 39
- Kumer, P., Narayan, R., & Johnson, J. L. 2008, Science

- Kuznetsov, A. V., & Mikheev, N. V. 1997, *Phys. Lett. B.*, 394, 123
- Kuznetsov, A. V., & Mikheev, N. V. 1999, *Mod. Phys. Lett. A.*, 14, 2531
- Lai, D. 1998, *ApJ*, 502, 721
- Lai, D., & Qian, Y.-Z. 1998, *ApJ*, 505, 844
- Lee, U. 1999, *ApJ*, 511, 359
- Lee, W. & Ramirez-Ruiz, E. 2007, *New J. Phys.*, 9, 17
- Lei, W. H. et al. 2009, *ApJ*, 700, 1970
- Li, J., Wickramasinghe, D. T., & Ruediger, G. 1996, *ApJ*, 469, 765
- Lightman, A. P., & Eardley, D. M. 1974, *ApJ*, 187, L1
- Liu, T., Gu, W. M., Xue, L., & Lu, J. F. 2007, *ApJ*, 661, 1025
- Long, M., Romanova M. M., & Lovelace R. V. E. 2007, *MNRAS*, 374, 436
- Long, M., Romanova, M. M., & Lovelace, R. V. E. 2008, *MNRAS*, 386, 1274
- Lovelace, R. V. E., Romanova, M. M., & Bisnovatyi-Kogan, G. S. 1995, *MNRAS*, 275, 244
- Lovelace, R. V. E., Wang, J. C. L., & Sulkanen, M. E. 1987, *ApJ*, 315, 504
- Luo, Q. H. 2005, *PASA*, 22, 157
- Lyubarsky, Y. E. 2009, *ApJ*, 698, 1570
- Lyubarsky, Y. E. 2009, *astro-ph*: 0909.4819
- MacFadyen, A. I., & Woosley, S. E. 1999, *ApJ*, 524, 262
- MacFadyen, A. I., Woosley, S. E., & Heger, A. 2001, *ApJ*, 550, 410
- Mazzali, P. A. et al. 2006, *Nature*, 442, 1018
- Metzger, B. D., Thompson, T. A., & Quataert, R. 2007, *ApJ*, 659, 561
- Metzger, B. D., Piro, A. L., & Quataert, E. 2008b, *MNRAS*, 390, 781
- Metzger, B. D., Thompson, T. A., & Quataert, E. 2008a, *ApJ*, 676, 1130
- Meyer, B. S., & Brown, J. S. 1997, *ApJS*, 112, 199

- Mikheev, N. V., & Narynskaya, E. N. 2000, *Mod. Phys. Lett. A.*, 15, 1551
- Miller, K. A., & Stone, J. M. 1997, *ApJ*, 489, 890
- Miller, W. A., George, N. D., Hheyfets, A., & McGhee, J. M. 2003, *ApJ*, 583, 833
- Nagataki, S., et al. 2006, *ApJ*, 647, 1255
- Nagataki, S., et al. 2007, *ApJ*, 659, 512
- Nagataki, S. 2009, *ApJ*, 704, 937
- Narayan R., Piran, T., & Kumar, P. 2001, *ApJ*, 557, 949
- Narayan, R., Paczyński, B., & Piran, T. 1992, *ApJ*, 395, L83
- Narayan, R., & Yi, I. 1994, *ApJ*, 428, L13
- Narayan, R., & Yi, I. 1995, *ApJ*, 444, 231
- Ostriker, E. C., & Shu, F. H. 1995, *ApJ*, 447, 813
- Popham, R., Woosley, S. E., & Fryer, C. 1999, *ApJ*, 518, 356
- Qian, Y.-Z., & Woosley, S. E. 1996, *ApJ*, 471, 331
- Romanova, M. M., Kulkarni, A. K., & Lovelace, R. V. E. 2008, *ApJL*, 673, 171
- Romanova, M. M., et al. 2005, *ApJ*, 635, L165
- Rosswog, S., Ramirez-Ruiz, E., & Davies, M. B. 2003, *MNRAS*, 345, 1077
- Ruderman, M. A., Tao, L., & Kluźniak, W. 2000, *ApJ*, 542, 243
- Ruffert, M., & Janka, H.-Th. 1998, *A&A*, 338, 535
- Ruffert, M., Janka, H.-Th., Takahashi, K., & Schäfer. G., 1997, *A&A*, 319, 122
- Ryu, D., Brown, G. L., Ostriker, J. P., & Loeb, A. 1995, *ApJ*, 452, 364
- Rigon, L., et al. 2003, *MNRAS*, 340, 191
- Riquelme, M., et al. 2005, *A&A*, 439, 427
- Roulet, E. 1998, *JHEP*, 980, 1013
- Shadmehri M., Khajenabi F., 2005, *MNRAS*, 361, 719

- Shakura, N. I., & Sunyaev, R. A. 1973, *A&A*, 24, 337
- Shapiro, S. L., & Teukolsky, S. A. 1983, *Black Holes, White Dwarfs, and Neutron Stars* (New York: Wiley)
- Shibata, M., & Taniguchi, K. 2006, *Phys. Rev. D*, 73, 064027
- Shu, F., et al. 1994, *ApJ*, 429, 781
- Soderberg, A. M. et al. 2006, *Nature*, 442, 1014
- Spruit, H. C., Daigne, F., & Drenkhahn, G. 2001, *A&A*, 369, 694
- Spruit, H., & Phinney, E. S. 1998, *Nature*, 393, 139
- Tchekhovskoy, A., McKinney, J. C., & Narayan, R. 2008, *MNRAS*, 388, 551
- Tchekhovskoy, A., McKinney, J. C., & Narayan, R. 2009, *ApJ*, 699, 1789
- Thompson, Todd A. 2003, *ApJL*, 585, 33
- Thompson, T. A., Burrows, A., & Meyer, B. S. 2001, *ApJ*, 562, 887
- Thompson, T. A., Chang, P., & Quataert, E. 2004, *ApJ*, 611, 380
- Tubbs, D. L., & Schramm, D. N. 1975, *ApJ*, 201, 467
- Usov, V. V. 1992, *Nature*, 357, 472
- Ustyugova, G. V. et al. 1999, *ApJ*, 516, 221
- Vietri, M., & Stella, L. 1998, *ApJ*, 507, 45L
- Vietri, M., & Stella, L. 1999, *ApJ*, 527, 43L
- Wang, Y.-M. 1995, *ApJ*, 449, 157L
- Wang, Z., Chakrabarty, D., & Kaplan, D. L. 2006, *Nature*, 440, 772
- Wheeler, J. C., Yi, I., Höflich, P., & Wang, L. 2000, *ApJ*, 537, 810
- Woosley, S. E. 1993, *ApJ*, 405, 273
- Woosley, S. E., & Bloom, J. S. 2006, *ARA&A*, 44, 507
- Xie, Y., Huang, C. Y., & Lei, W. H. 2007, *ChJAA*, 7, 685

Xie, Y. et al. 2009, MNRAS, 398, 583

Yakovlev, D. G., Kaminker, A. D., Gnedin, O. Y., & Haensel, P. 2001, Phys. Rep., 354, 1

Yu, Y. W., & Dai, Z. G. 2007, A&A, 470, 119

Yuan, Y. F., & Zhang, J. L. 1998, A&A, 335, 969

Zhang, B., & Mészáros, P. 2001, ApJ, 552, 35

Zhang, D., & Dai, Z. G. 2008a, ApJ, 683, 329 (paper I)

Zhang, D., & Dai, Z. G. 2008b, MNRAS, 388, 1409

Zhang, D., & Dai, Z. G. 2009, ApJ, 703, 461 (paper II)

Disk Heating Rate and Maximum Outflow Energy Rate

	Disk Heating Energy Rate ( $10^{51}$ erg $s^{-1}$ )			Max Outflow Energy Rate ( $10^{51}$ erg $s^{-1}$ )		
	$B_0 = 10^{15}$ G	$B_0 = 10^{16}$ G	$B_0 = 10^{17}$ G	$B_0 = 10^{15}$ G	$B_0 = 10^{16}$ G	$B_0 = 10^{17}$ G
$\xi=0.2$	29.3	25.9	8.08	8.60	8.63	1.45
$\xi=0.6$	18.3	15.7	6.47	19.5	18.8	3.07
$\xi=0.9$	13.5	11.7	5.53	24.4	22.9	4.01

Table 1: The disk heating rate is calculated in the region outside the Alfvén radius, where differential rotation and viscosity are significant:  $\dot{E}_{\text{heat}} = \int_{r_A}^{r_{\text{out}}} 2\pi r dr$ . Here the outflow index  $\xi = 0.2, 0.6, 0.9$ , and the accretion rate  $\dot{M} = 0.5M_{\odot} s^{-1}$ . The max thermally-driven energy rate is estimated using equation (47). The total thermal outflow energy can be considered as 0.1 – 1 fraction of the maximum energy, as discussed in paper II.

Disk Properties Depending on Magnetar Field Strength

$B_0 \sim 10^{14}$ G	no funnel accretion, disk is similar to that without fields
$B_0 \sim 10^{15}$ G	no funnel accretion, MHD coupling is important in the disk inner region, thermal outflow
$B_0 \sim 10^{16}$ G	weak funnel accretion, disk is denser, hotter with higher pressure, brighter $L_{\nu\bar{\nu}}$ from the disk, thermal outflows from $r > r_A$ , magnetic winds inside
$B_0 \sim 10^{17}$ G	strong funnel accretion, but no shock, much brighter $L_{\nu\bar{\nu}}$ from the stellar “hot spot”, magnetically-dominated wind significantly

Table 2: The accretion rate near the Alfvén radius  $r_A$  or the stellar surface  $r_*$  (depending on  $r_A > r_*$  or  $r_A < r_*$  respectively) is  $\dot{M} = 0.1M_{\odot} s^{-1}$ . The neutrino cooling emission is efficient in this case, and the accretion flow is an NDAF. The inner region satisfying the self-similar structure (papers I and II) can be ignored even the disk is similar to that without fields.

Values of  $\Delta\Omega/2\pi$  on Magnetar Surface Based on the First Scenario

$\delta/r_*$	$r_m/r_*(\Theta = 90^\circ)$			$r_m/r_*(\Theta = 75^\circ)$		
	2	4	7	2	4	7
0.1	1.84e-2	6.38e-3	2.74e-3	1.77e-2	6.16e-3	2.64e-3
0.5	0.110	3.46e-2	1.43e-2	0.106	3.34e-2	1.38e-2
1	0.292	7.74e-2	3.02e-2	0.282	7.48e-2	2.92e-2
2	-	0.208	0.070	-	0.200	6.70e-2

Table 3: The ratio of the solid angle of the “hot spot” ring-like belt  $\Delta\Omega$  formed by funnel accretion to the half total solid angle  $2\pi$  based on the first scenario in Append B, in which the accreted matter onto the ring-like belt of “hot spot” is from the region between the magnetosphere edge  $r_m$  and the Alfvén radius  $r_A$ . We take  $\delta/r_*$  from 0.1 to 2, and  $r_m/r_*$  from 2 to 7. Here the left three columns are for  $\Theta = 90^\circ$  and the right three ones are for  $\Theta = 75^\circ$ . The typical value of  $\Delta\Omega$  is around  $10^{-2}$ .

Values of  $\Delta\Omega/2\pi$  on Magnetar Surface Based on the Second Scenario

$H/r_m$	$\Theta = 90^\circ (r_A/r_*)$			$\Theta = 75^\circ (r_A/r_*)$		
	2	4	7	2	4	7
0.1	5.28e-3	3.74e-3	2.82e-3	5.50e-3	3.62e-3	2.72e-3
0.3	4.60e-2	3.26e-2	2.46e-2	4.44e-2	3.14e-2	2.38e-2
0.5	0.120	8.50e-2	6.42e-2	0.116	8.22e-2	6.20e-2

Table 4: The ratio of the solid angle of the “hot spot” ring-like belt  $\Delta\Omega$  to the total solid angle  $2\pi$  based on the second scenario in Append B, in which the accreted matter onto the ring-like belt of “hot spot” is from the disk vertical section surface at  $r = r_m$ . We take the disk thickness at this radius as  $H/r_m = 0.1, 0.3, 0.5$ , and  $r_m/r_*$  also from 2 to 7. The typical value of  $\Delta\Omega$  is still around  $10^{-3} - 10^{-2}$  in this scenario.

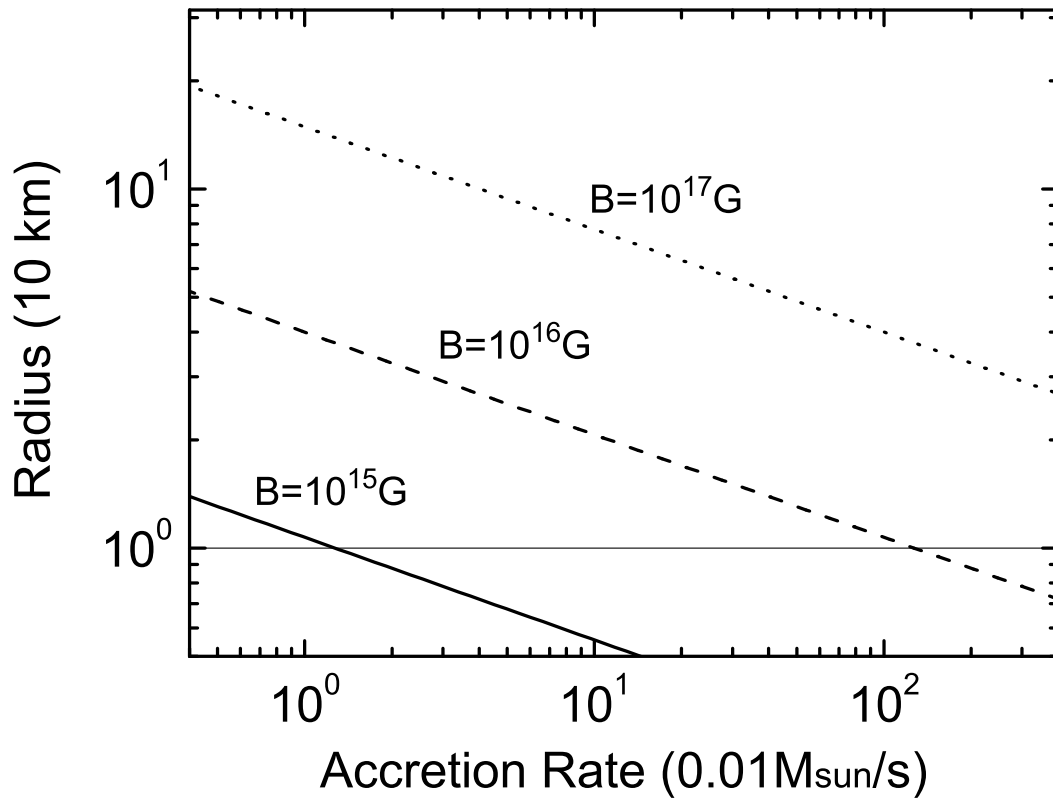


Fig. 1.— Alfvén radius  $r_A$  as a function of accretion rate in hyperaccreting disks. We take the magnetar field as  $10^{15}$ ,  $10^{16}$  and  $10^{17}$  G.

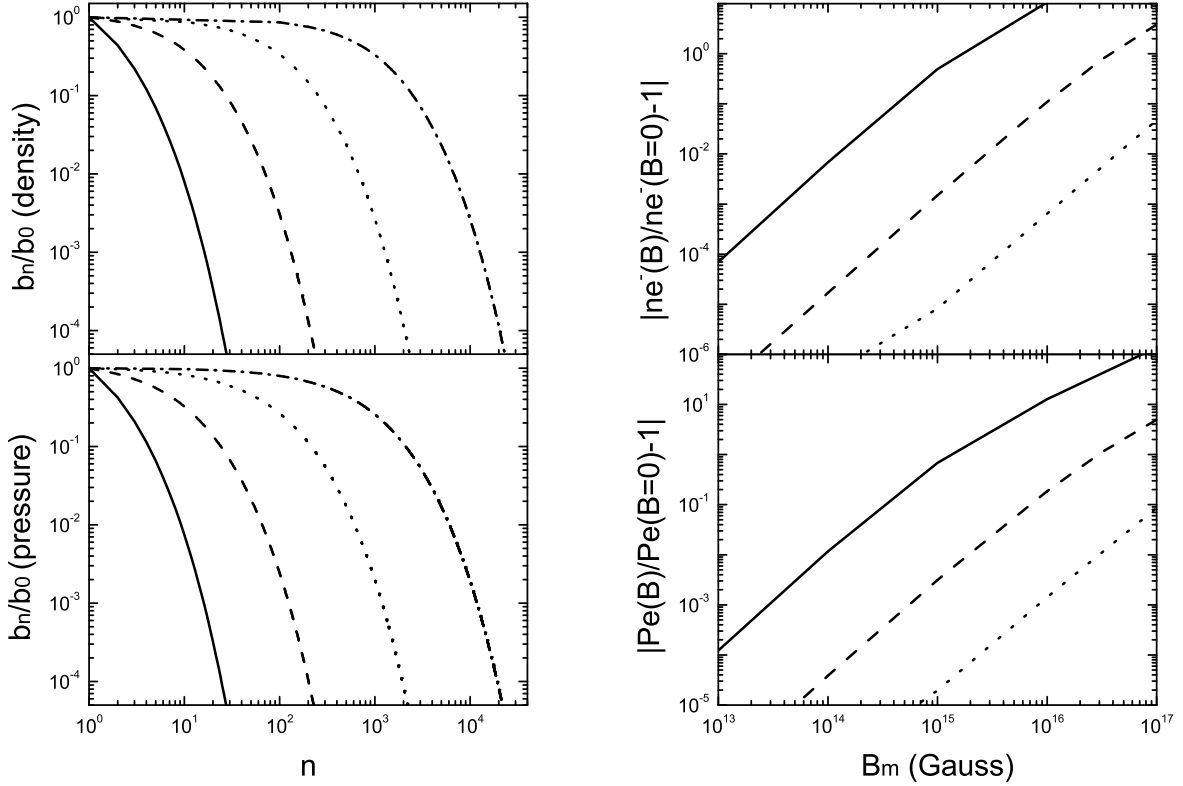


Fig. 2.— *Left*: Convergence performance of Landau level series of electron density and pressure with different magnetic fields  $B = 10^{16}$  G (*solid line*),  $10^{15}$  G (*dashed line*),  $10^{14}$  G (*dotted line*) and  $10^{13}$  G (*dash-dotted line*) and temperature  $T = 5 \times 10^{10}$  K and chemical potential  $\eta_e = 1$ , where  $b_n$  is the  $n$  term in the density and pressure series (5) and (8). *Right*: Comparison of density and pressure with and without magnetic fields with temperature  $T = 10^{10}$  K (*solid line*),  $5 \times 10^{10}$  K (*dashed line*) and  $2 \times 10^{11}$  K (*dotted line*).

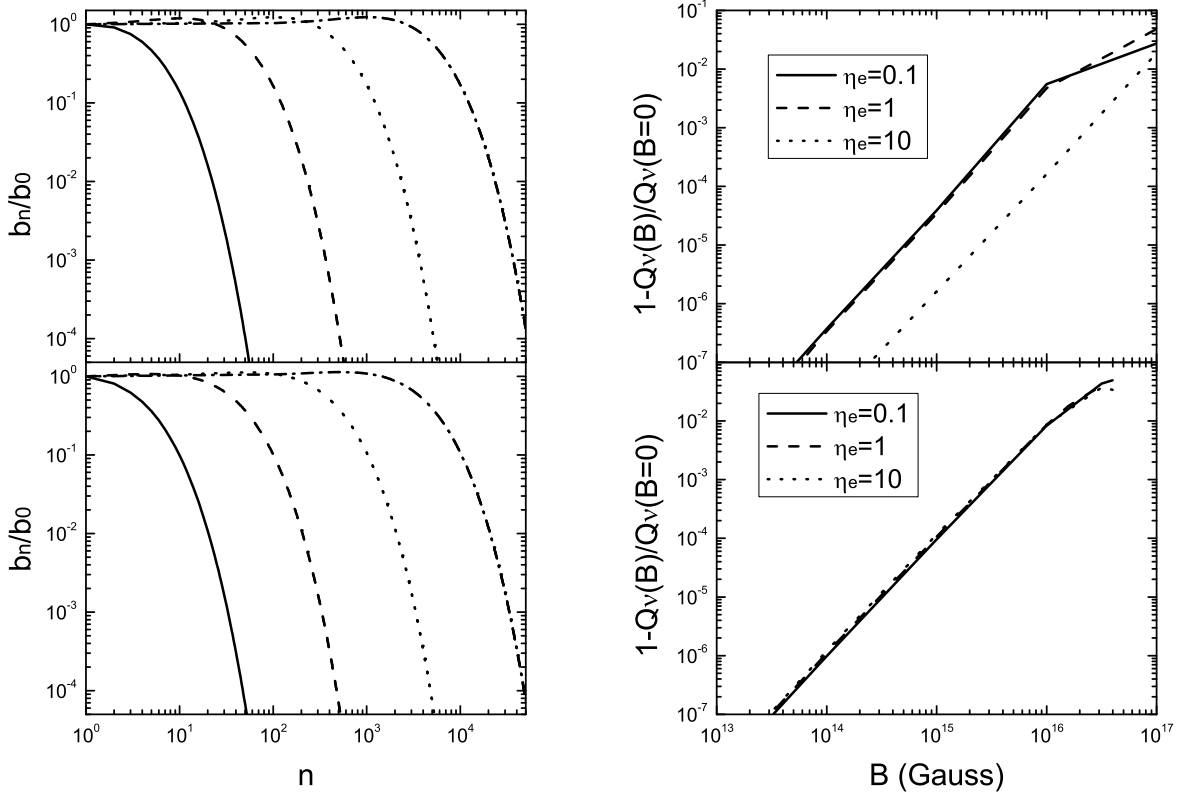


Fig. 3.— *Left*: Convergence performance of Landau level series of neutrino cooling with different magnetic fields. Upper one for the cooling rate  $\dot{q}_{p+e^- \rightarrow n+\nu_e}$  and lower for  $\dot{q}_{n+e^+ \rightarrow p+\bar{\nu}_e}$ , where temperature  $T = 5 \times 10^{10}$  K and chemical potential  $\eta_e = 1$  is adopted. Lines are as in Fig. 1. *Right*: Comparison of neutrino cooling rates with and without magnetic fields. Temperature  $T = 5 \times 10^{10}$  K and  $\eta_e = 0.1, 1$  and 10. Also, upper is for  $\dot{q}_{p+e^- \rightarrow n+\nu_e}$  and lower for  $\dot{q}_{n+e^+ \rightarrow p+\bar{\nu}_e}$ .

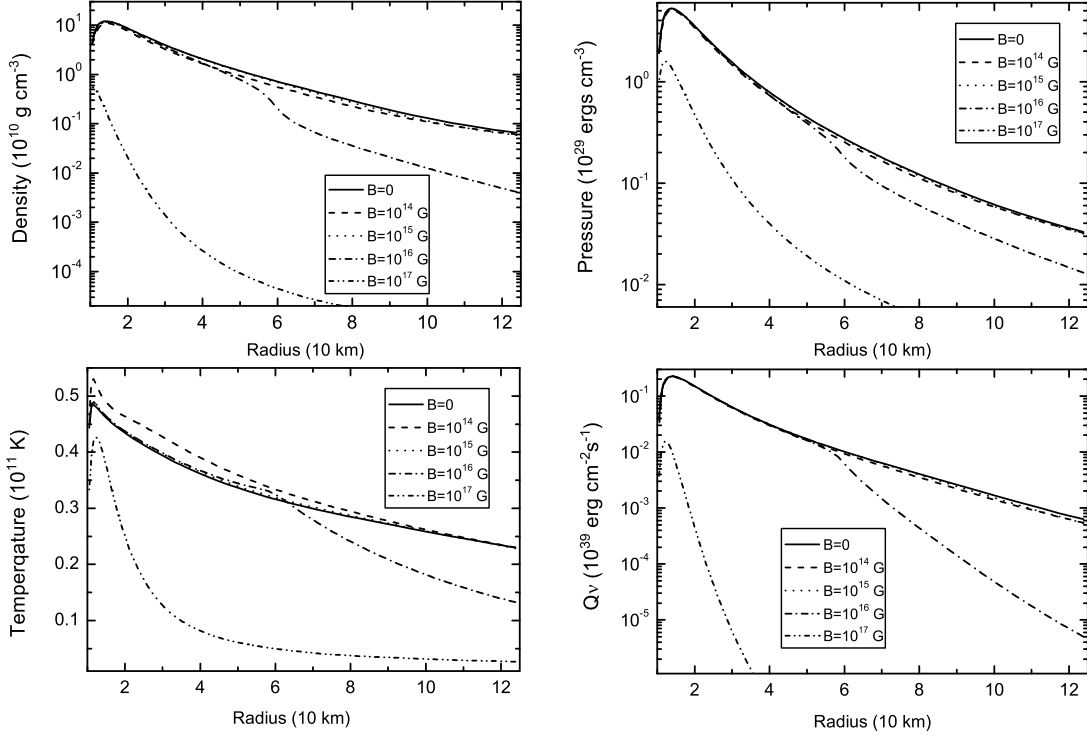


Fig. 4.— Quantum effects of microphysics and thermodynamics in strong magnetic fields to affect the disk properties. In order to see the effects clearly, we still take the non-magnetized conservation equations (i.e., (A8), (A10) to (A14) in Appendix A), and only change a set of equations of state in Section 2. Also, we take the magnetic field as uniform  $B = 10^{14}, 10^{15}, 10^{16}, 10^{17} \text{ G}$  and without field, the accretion rate  $\dot{M} = 0.1M_{\odot} \text{ s}^{-1}$ .

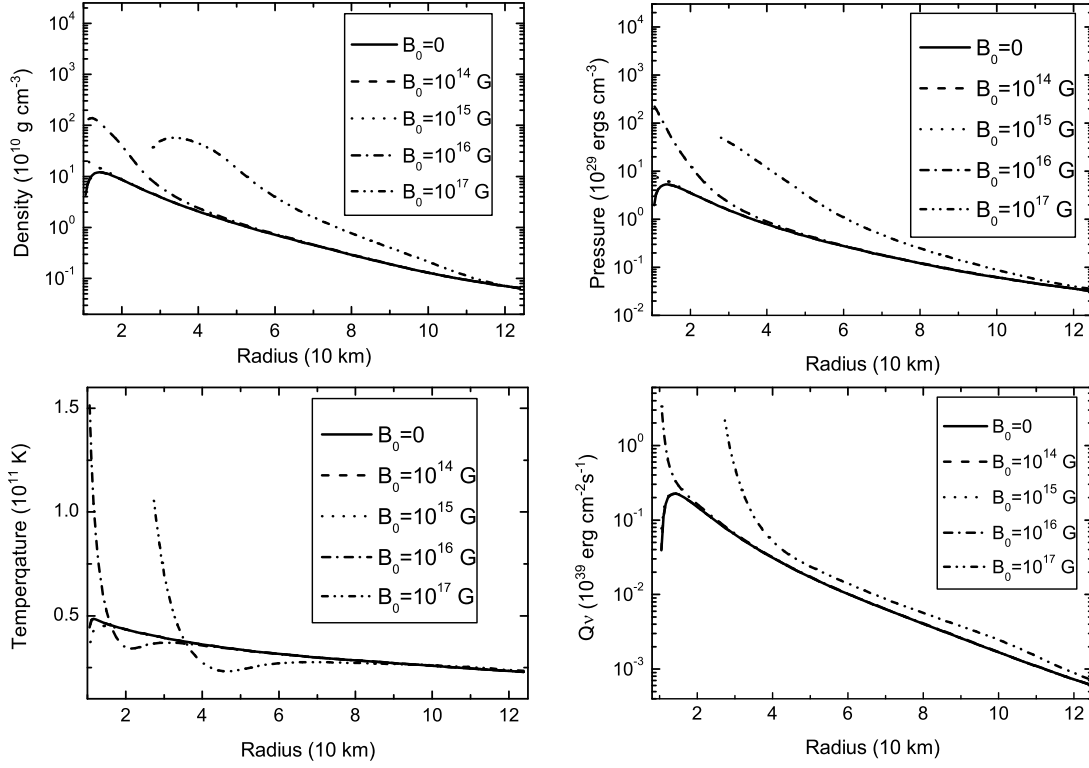


Fig. 5.— Effects of strong magnetic field coupling on angular momentum transfer and heating via Joule dissipation on the disk. We do not consider the field quantum effects as discussed in Section 2, but only adopt the MHD equations in Section 3. The magnetic field topology is dipolar, and an open configuration with parameter  $\beta = 0.6$ , angular velocity ratio  $s = 1$ , and  $B_0 = 10^{14}, 10^{15}, 10^{16}, 10^{17}$  G. The accretion rate is the same as in Figure 4.

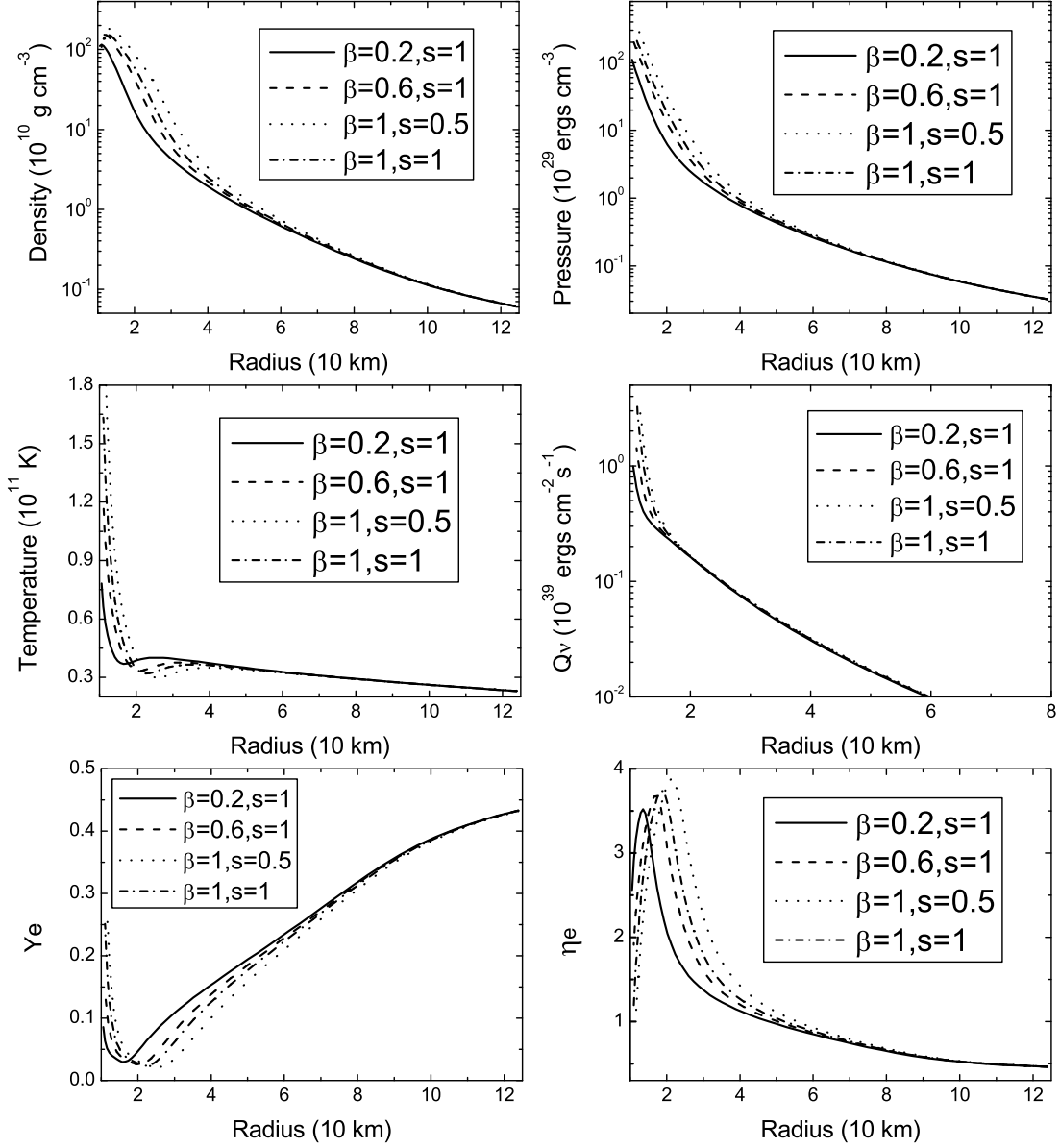


Fig. 6.— Disk structure with  $\dot{M} = 0.1M_{\odot} \text{ s}^{-1}$  for the magnetar surface vertical field  $B_0 = 10^{16} \text{ G}$ . The magnetic field in the disk is open with parameter  $\beta = 0.2, 0.6, 1$  and disk angular velocity  $s = 0.5, 1$ .

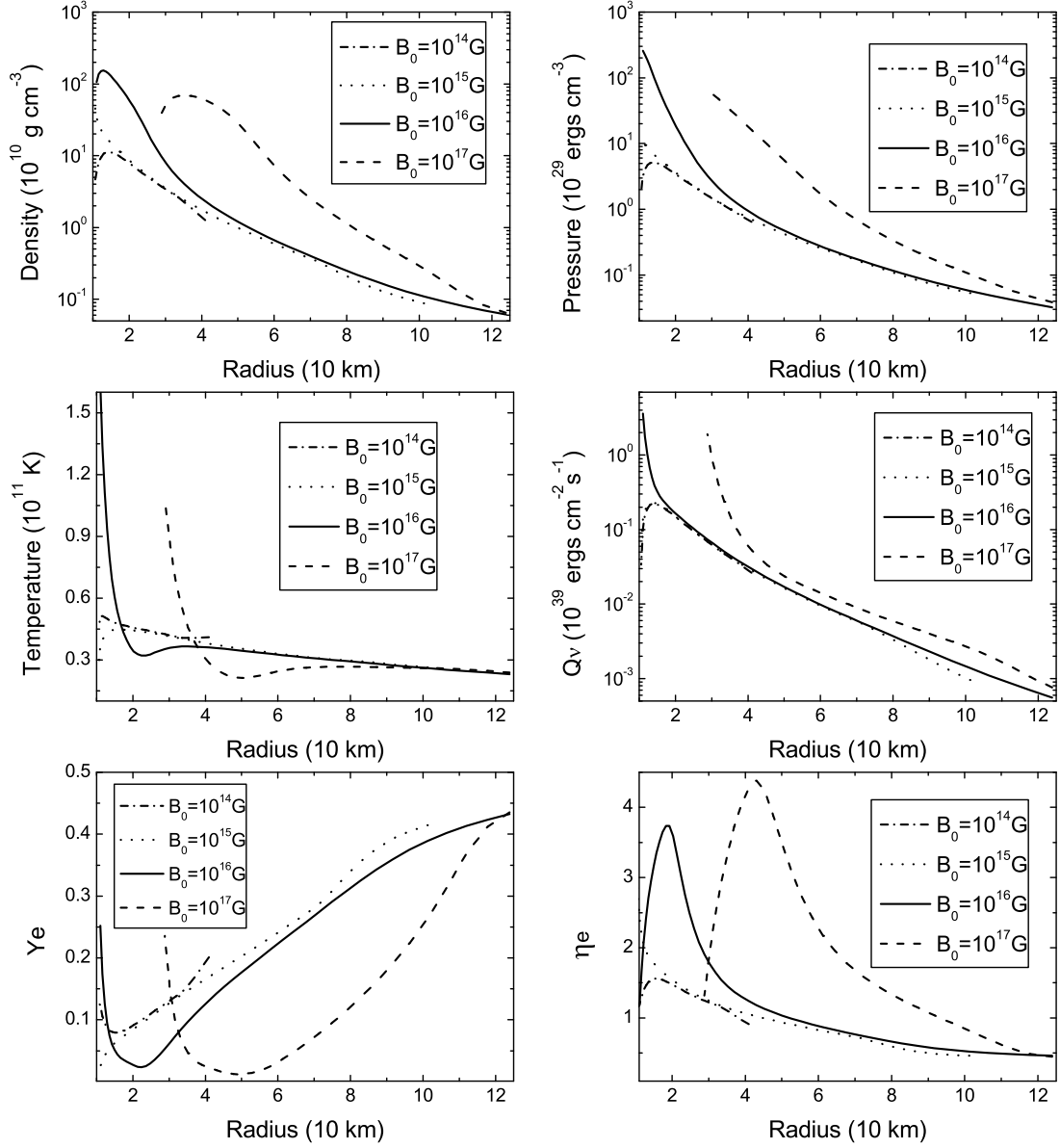


Fig. 7.— Disk structure with  $\dot{M} = 0.1M_\odot \text{ s}^{-1}$  for the magnetar surface vertical field  $B_0 = 10^{14}, 10^{15}, 10^{16}$  and  $10^{17}$  G, where the magnetic field in the disk is in an open configuration with  $\beta = 1$  and  $s = 1$ .

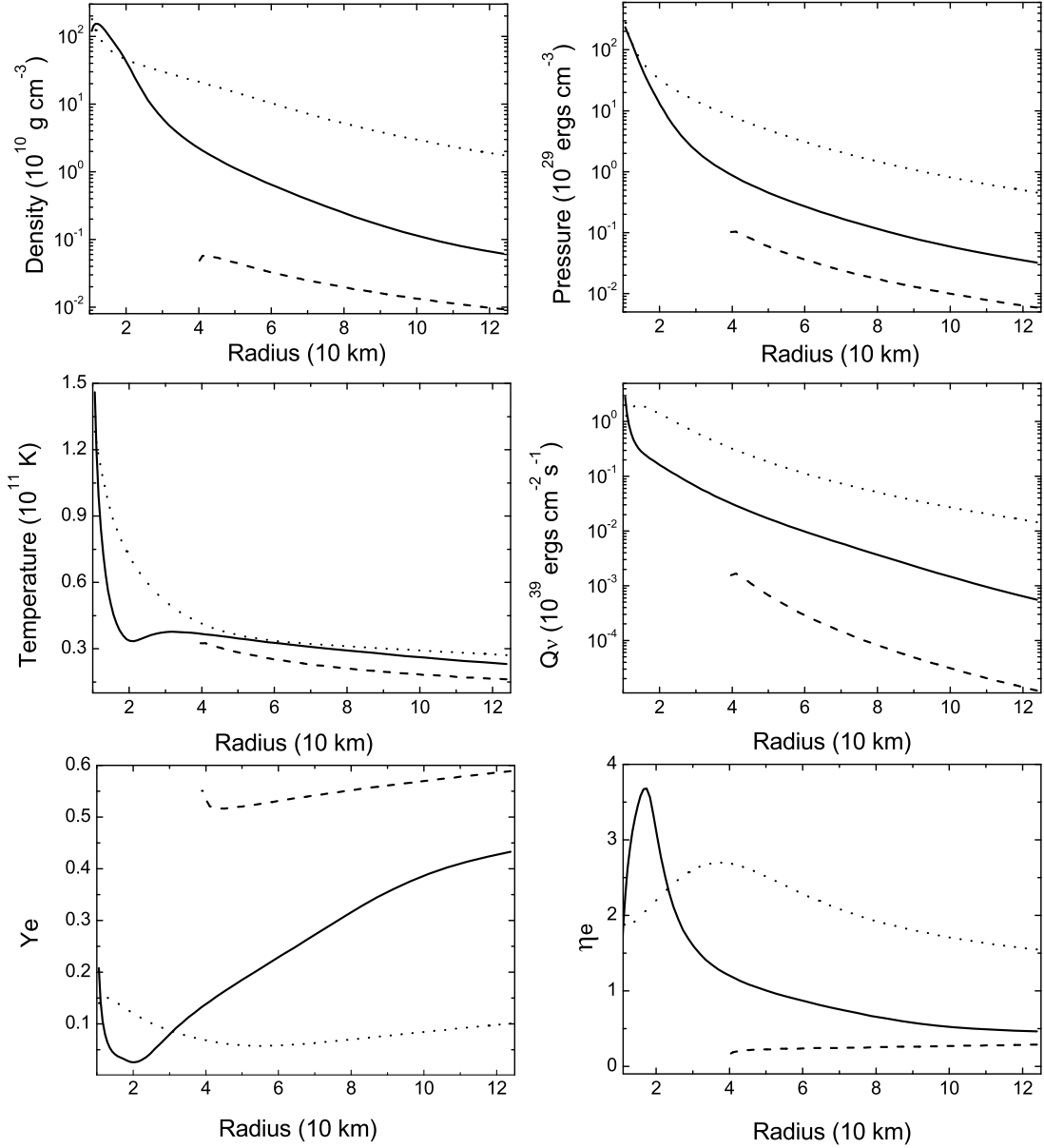


Fig. 8.— Disk structure for different disk accretion rate  $\dot{M} = 0.02$  (*solid line*),  $0.1$  (*dashed line*) and  $1 M_{\odot} \text{ s}^{-1}$  (*dotted line*) with open disk field  $\beta = 0.6$  and  $s = 1$ , while the surface vertical field  $B_0 = 10^{16} \text{ G}$ .

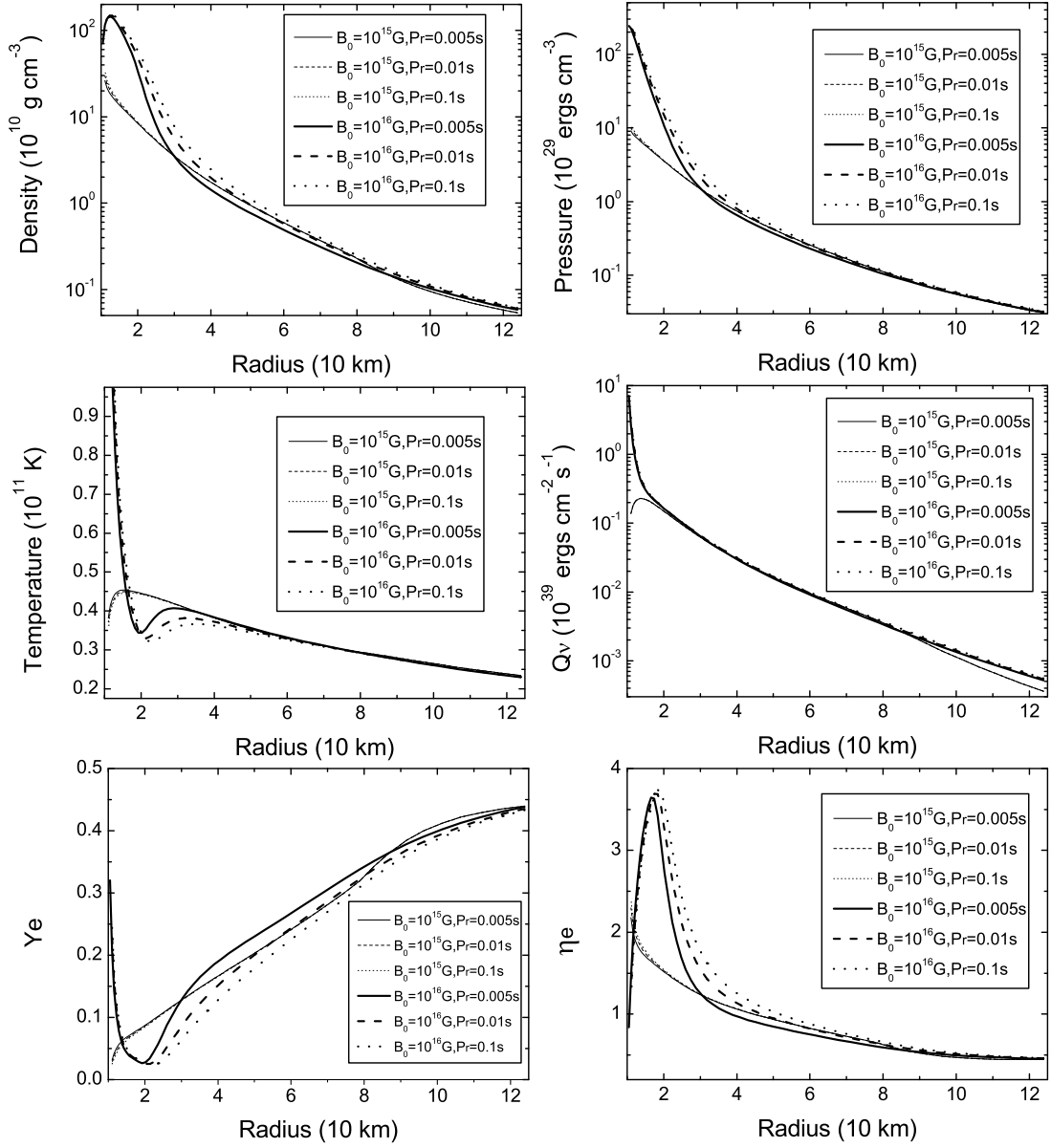


Fig. 9.— Disk structure with  $\dot{M} = 0.1M_{\odot} \text{ s}^{-1}$  for the surface vertical field  $B_0 = 10^{15}, 10^{16}$  G, the disk magnetic field is closed with  $\beta \simeq 1$ ,  $s = 1$ . The period of a central magnetar  $P_r = 0.005, 0.01$  and  $0.1$  sec.

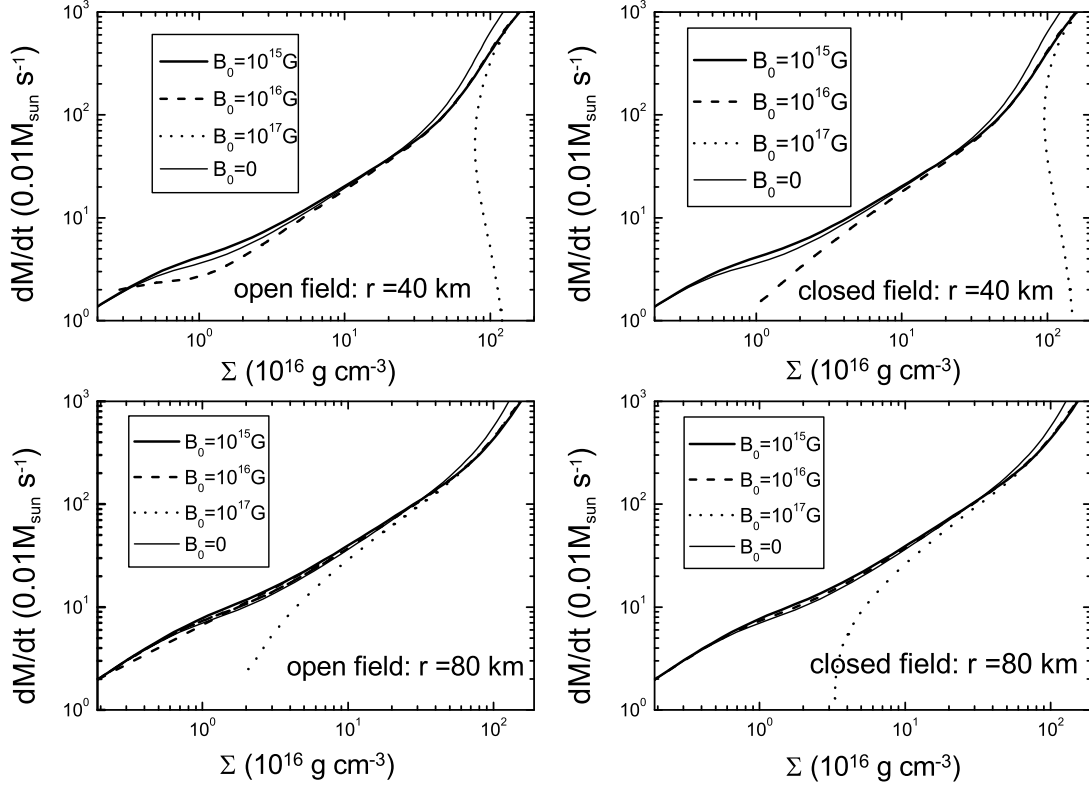


Fig. 10.—  $\dot{M} - \Sigma$  curves for given disk radius  $r = 40$  and  $80$  km. In the case of an open disk field we take  $\beta = 0.6$  and  $s = 1$ ; while in the case of a closed disk field we take  $\beta = 1$ ,  $s = 1$  and  $P_r = 100\text{ms}$ .

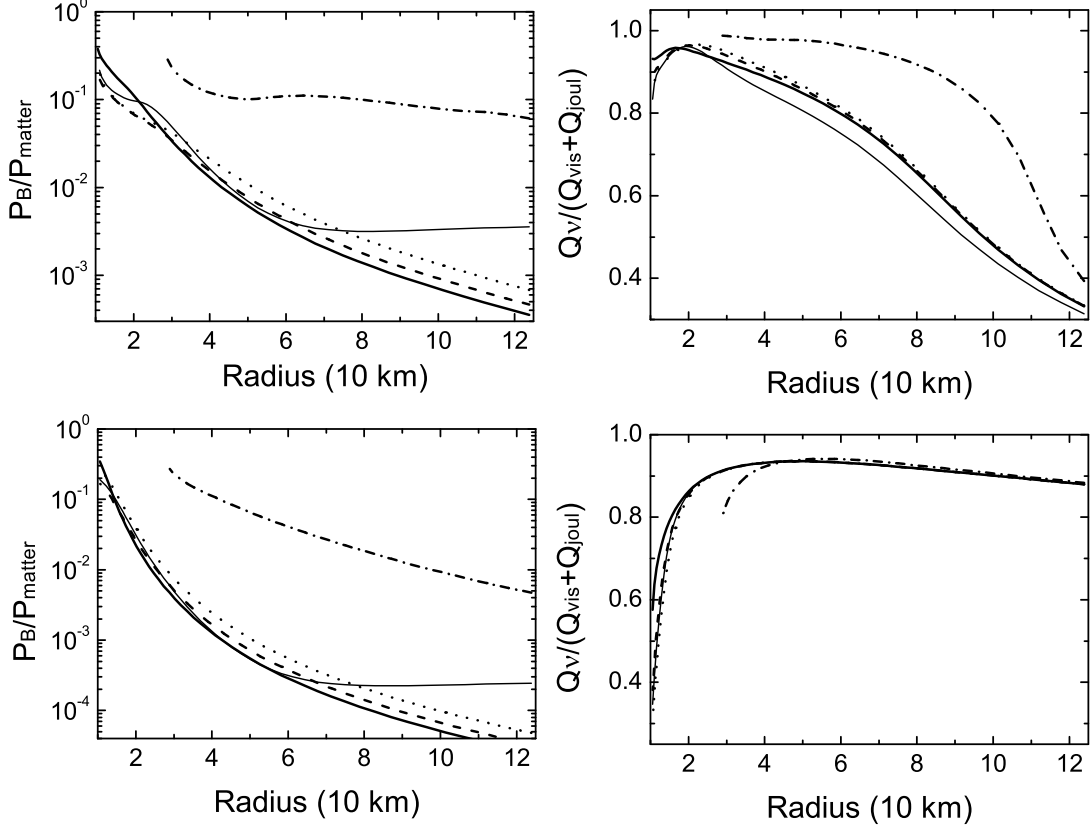


Fig. 11.— Ratio of magnetic pressure  $P_B$  to the accretion matter  $P_{\text{matter}}$ , and ratio of neutrino emission  $Q_{\nu}^{-}$  to the local heating rate  $Q_{\text{vis}}^{+} + Q_{\text{joul}}^{+}$  as functions of disk radius. Upper two panels for the accretion rate  $M_{\odot} = 0.1 M_{\odot} \text{ s}^{-1}$ . Open disk field with  $B_0 = 10^{16} \text{ G}$ ,  $\beta = 0.2, s = 1$  (*thick solid line*),  $\beta = 0.6, s = 1$  (*thick dashed line*),  $\beta = 1, s = 1$  (*thick dotted line*),  $B_0 = 10^{17} \text{ G}$ ,  $\beta = 1, s = 1$  (*thick dot-dashed line*) and closed field with  $\beta = 1, s = 1, P_r = 0.005 \text{ s}$  (*thin solid line*). Bottom two panels for the accretion rate  $M_{\odot} = 1 M_{\odot} \text{ s}^{-1}$ , and the lines are the same as the upper panels.

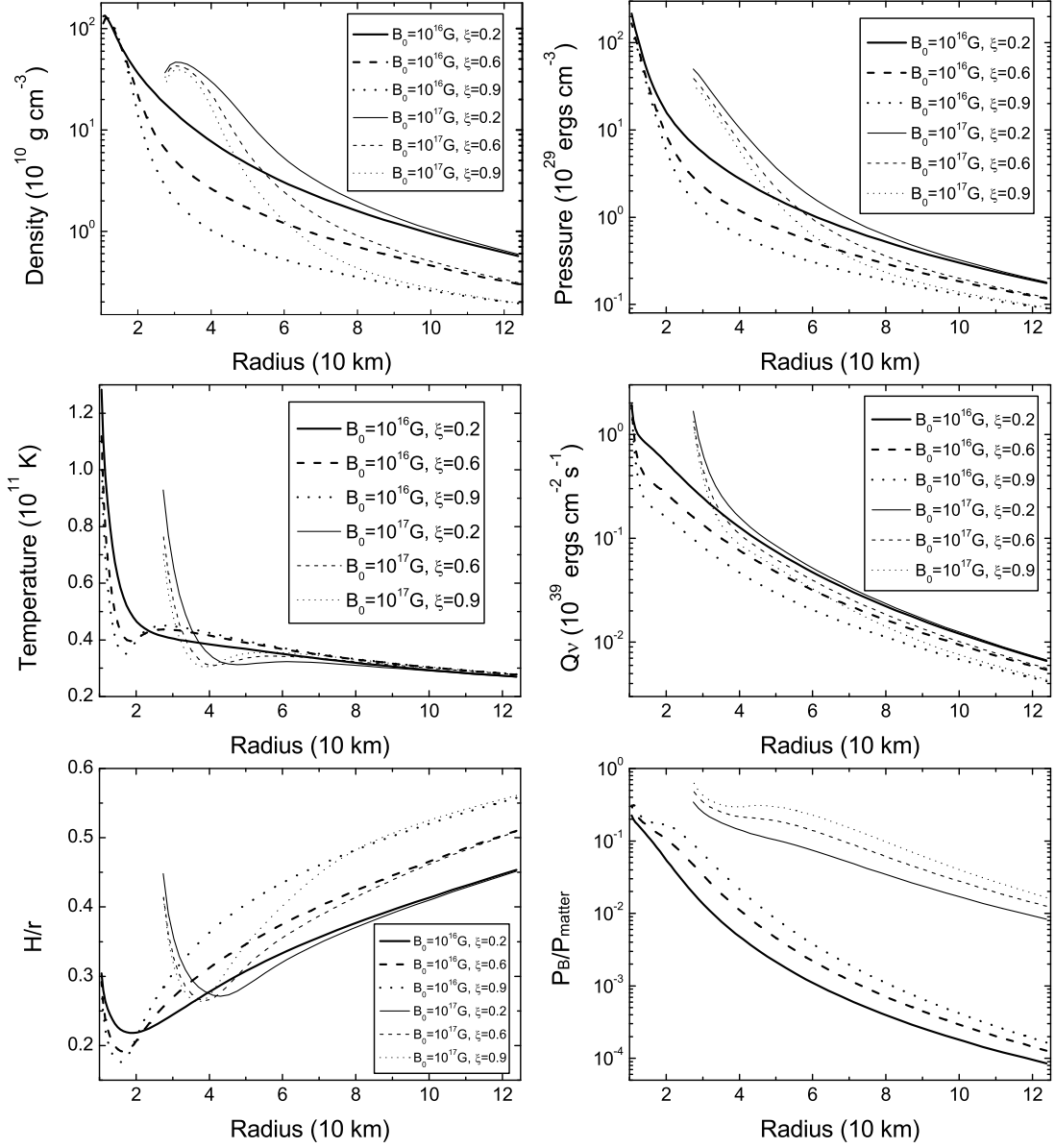


Fig. 12.— Disk structure and luminosity for three values of outflow index  $\xi = 0.2, 0.6, 0.9$  with the open disk field  $\beta = 0.6, s = 1, B_0 = 10^{16}, 10^{17} \text{ G}$ . We give an initial accretion rate  $\dot{M} = 0.5M_{\odot} \text{ s}^{-1}$  at the outer radius  $r = 124 \text{ km}$ .

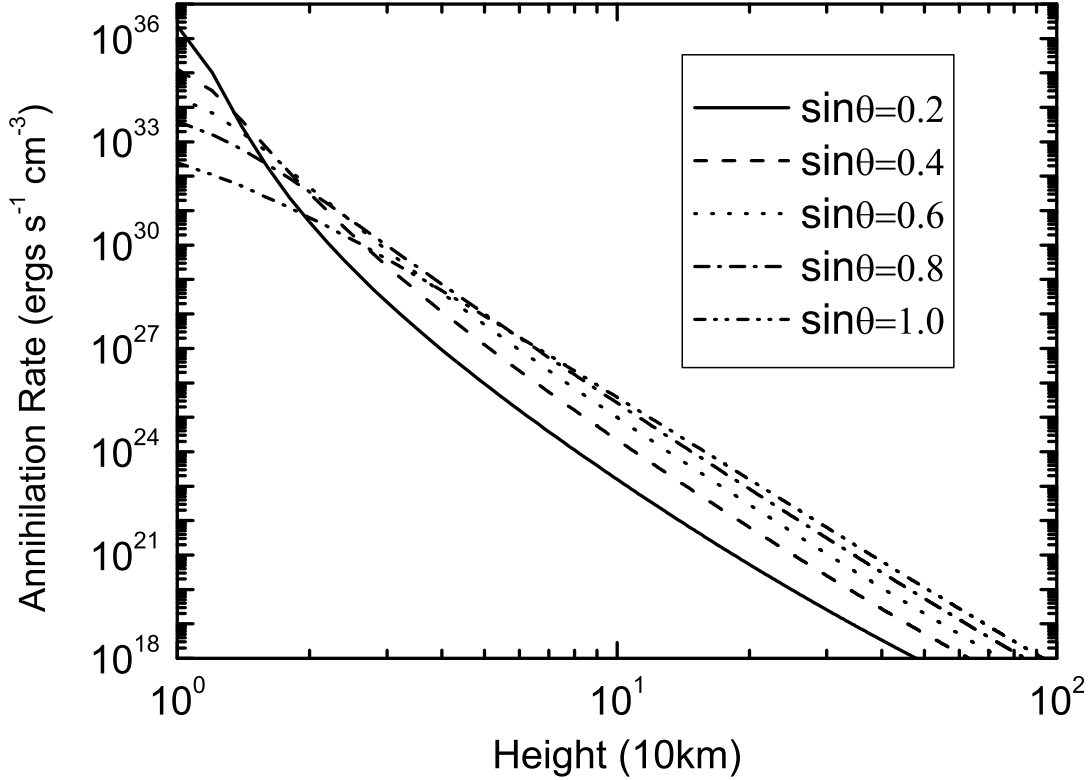


Fig. 13.— The neutrino annihilation rate  $l_{\nu\bar{\nu}}$  ( $\text{erg s}^{-1} \text{cm}^{-3}$ ) along the stellar magnetic pole as a function of height, where the values of  $\sin\theta \simeq \sqrt{r_*/r_A}$  are taken as  $\sin\theta = 0.2, 0.4, 0.6, 0.8, 1.0$ ,  $\Delta\Omega/2\pi = 10^{-2}$ , accretion rate  $\dot{M} = 0.5M_\odot \text{ s}^{-1}$ , and the energy release efficiency  $\epsilon = 0.5$ . The integrated annihilation energy along the pole is  $\int_{r_*}^{\infty} l_{\nu\bar{\nu}} dz = 4.95 \times 10^{41}, 3.31 \times 10^{40}, 5.92 \times 10^{39}, 1.31 \times 10^{38}$  and  $9.21 \times 10^{37} \text{ erg s}^{-1} \text{cm}^{-2}$  for the value of  $\sin\theta = 0.2, 0.4, 0.6, 0.8$  and  $1.0$  respectively.

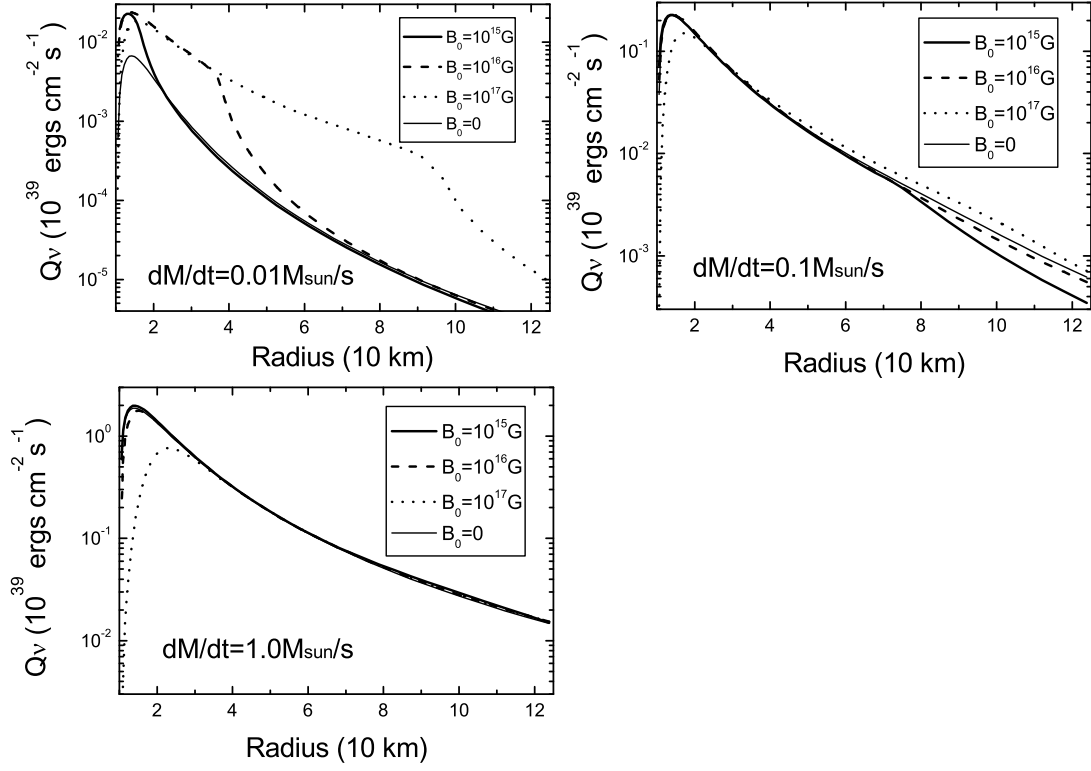


Fig. 14.— Neutrino luminosity for accretion rate  $\dot{M} = 0.01, 0.1$  and  $1 M_\odot \text{ s}^{-1}$  and magnetar surface field  $B_0 = 10^{15}, 10^{16}$  and  $10^{17} \text{ G}$  without Joule dissipation in the disk. The open field model is adopted with  $\beta = 0.6$  and  $s = 1$ .